Turicibacter strains differentially modify bile acids and host lipids

Jonathan B. Lynch[1§]*, Erika L. Gonzalez[1], Kayli Choy[1], Kym F. Faull[2,3,4], Talia Jewell[5], Abelardo Arellano[5], Jennifer Liang[5], Kristie B. Yu[1], Jorge Paramo[1], Elaine Y. Hsiao[1]

[1]Department of Integrative Biology & Physiology, University of California Los Angeles, Los Angeles, CA 90095, USA

[2]Department of Psychiatry and Biobehavioral Sciences, University of California Los Angeles, Los Angeles, CA 90095, USA

[3]Jane and Terry Semel Institute for Neuroscience and Human Behavior, University of California Los Angeles, Los Angeles, CA 90095, USA

[4]Pasarow Mass Spectrometry Laboratory, University of California Los Angeles, Los Angeles, CA 90095, USA

[5]Isolation Bio, San Carlos, CA 94070, USA

[§]Current address: Department of Biological Chemistry, Johns Hopkins University, Baltimore, MD , USA

*Correspondence to: jlynch48@jhmi.edu

ABSTRACT

Bacteria from the *Turicibacter* genus are prominent members of the mammalian gut microbiota and are associated with alterations in dietary fat and body weight, but the specific connections between these symbionts and host physiology are poorly understood. We genomically and phenotypically characterized a diverse set of mouse- and human-derived *Turicibacter* strains, and found they group into three clades that differ in their transformations of bile acids. We identified *Turicibacter* bile salt hydrolases that confer strain-specific differences in bile deconjugation. Colonization with individual *Turicibacter* strains led to changes in host bile acid profiles, generally aligning with those produced *in vitro*. Further, colonizing mice with another bacterium expressing bile-modifying genes from these strains decreased serum cholesterol and triglycerides, as well as adipose tissue mass. This work identifies genes that enable diverse *Turicibacter* strains to differentially modify host bile acids and lipid metabolism, and positions multiple *Turicibacter* strains as candidates for altering host fat biology.

34 **MAIN TEXT**

35

36 ***Introduction***

37

38 The gut microbiota forms complex relationships with its host organism, modulating broad
39 aspects of host physiology including metabolism[1,2] and neurobiology[3,4]. Often, the connections
40 between the gut microbiota and host physiology are easiest to decipher through presence/absence
41 of large sectors of the microbial community (examples in [5–7]), but in some cases, specific
42 microbial features and/or taxa serve important roles in host physiology[8–10].

43 The bacterium *Turicibacter sanguinis* is the best-studied species of the *Turicibacter*
44 genus, which is prevalent in the gut microbiota of several animals, including humans[11], mice[7],
45 cows[12], pigs[13], and chickens[14]. *Turicibacter* can reach relative abundances of >20% in the rodent
46 small intestine[15] and 0.5% in the human fecal microbiota[16,17]. A study of 1126 sets of twins
47 found *Turicibacter* was a highly heritable taxon in the human fecal microbiota[18], supporting
48 associations between *Turicibacter* abundance and host genetics found in Diversity Outbred
49 mouse collections[19–21]. Long-standing co-evolutionary connections between this taxon and
50 humans are suggested by the high abundance of *Turicibacter* sequences that have been measured
51 in ancient and non-industrial human gut microbiotas[17,22–24].

52 The mammalian gut microbiota has long been associated with obesity[25,26], but studies
53 often provide strong correlations rather than mechanistic determinants of these relationships,
54 indicating a further need for fundamental interrogation into connections between the microbiota
55 and host fat[27]. Numerous microbiota community profiling studies reveal correlations between
56 *Turicibacter* and features of host fat metabolism, such as adiposity and dietary lipids[28–33], but the
57 nature of these correlations varies[34,35]. We recently observed that the type strain of *T. sanguinis,*
58 MOL361[36,37], broadly alters the host serum lipidome while decreasing serum triglycerides in

59 mice[38]. This same strain was also reported to modify bile species through deconjugation and
60 dehydrogenation *in vitro*[21], suggesting at least one potential means by which *Turicibacter* can
61 influence host lipid status. Based on these findings, we hypothesized that there may be variations
62 in the functional activity of *Turicibacter* strains that account for differences in host bile and lipid
63 biology, providing a mechanism to connect this taxon to aspects of host physiology.
64
65 ***Results***
66
67 Turicibacter *isolates separate into genetically distinguishable strains*
68
69 To better understand the diversity within the *Turicibacter* genus, we gathered nine
70 isolates from the fecal microbiotas of mice and humans that had been identified as *T. sanguinis*
71 based on their 16S rRNA gene sequence (97% full length 16S rRNA gene sequence similarity
72 cutoff, **Supplementary Table 1**). Two of these isolates had been previously identified (human-
73 derived type strain MOL361 and H121, which was derived from contaminated germ-free
74 mice[36,39]); five had been isolated but not published (human isolates 18F6, T46, and T129, and
75 mouse isolates 1E2 and TA25); and two were isolated from a human fecal sample specifically
76 for this study (GALT-E2 and GALT-G1) using an array-based isolation and cultivation platform
77 (see Methods). We performed shotgun short read sequencing and created draft assemblies of
78 each isolate genome. Comparisons of the 16S rRNA gene phylogeny (**Fig. 1a**), general genome
79 characteristics (**Fig. 1b**), or specific genome sequence (**Fig. 1c, d**) revealed that even with this
80 fairly small sample of the 16S rRNA gene-based "*T. sanguinis*" species designation, there were
81 at least three distinct subgroups: two from humans (exemplar isolates MOL361 and H121, with
82 99.3% full length 16S rRNA gene similarity), and one from mice (exemplar strain 1E2, 97.5%
83 and 97.8% 16S rRNA gene similarity with MOL361 and H121, respectively). Genomic

84 alignments indicated a substantial amount of shared DNA sequences within members of the
85 same subgroups (all within group average nucleotide identity [ANI] >98.3%) with the remaining
86 amount of genetic variation indicating smaller genetic differences between related isolates. These
87 within-subgroup shared sequences were distinct from members of the other two subgroups
88 (intergroup ANI: MOL361-H121=76.80%, MOL361-1E2=74.95%, H121-1E2=77.43%). It is
89 important to note that the H121-group genomically resembles the newly described species
90 *Turicibacter bilis*[13] (98.8% ANI), currently the only other named species from this genus.
91 Overall, these genomic differences suggest distinct evolutionary histories that correspond at least
92 partially with host origin.
93
94 Turicibacter *isolates differ in their impact on host fat biology and circulating metabolome*
95
96 Previous findings revealed that monocolonizing mice with *T. sanguinis* MOL361 altered
97 host fat tissue and circulating lipids[38]. Due to the large genomic variation between our
98 *Turicibacter* strains, we predicted that they would vary in their effects on host lipid biology. We
99 chose representative isolates from each of the distinct phylogenetic subgroups (MOL361, H121
100 and T129, and 1E2) and measured their effects on circulating metabolites and adipose tissue in
101 monocolonized mice relative to germ-free (GF) and conventionalized controls (*i. e.* gavaged with
102 complete microbiota, CONV). Compared to GF mice, CONV mice had decreased levels of
103 several dicarboxylate fatty acids, long-chain fatty acids, and long-chain acyl carnitines, with a
104 broad increase in short- and medium-chain acyl carnitines (**Fig. 2a**). Consistent with a previous
105 report[38], colonization with individual *Turicibacter* strains also induced widespread alterations in
106 host serum lipids, with several strain-level differences in host lipid alterations (**Fig. 2a,**
107 **Supplementary Table 2**). Compared to GF controls, MOL361 increased a subset of long-chain
108 acyl carnitines, and decreased many long-chain saturated fatty acids. In addition, colonization

109 with MOL361 elicited trending decreases in host cholesterol to levels below those seen in GF
110 (**Fig. 2b**). Compared to GF, H121 colonization significantly increased serum levels of several
111 medium-chain fatty acids, dicarboxylic acids, and short-, medium- and long-chain acyl
112 carnitines. 1E2 colonization had a smaller overall effect on host lipids, but led to a decrease in
113 several dicarboxlyate fatty acids (**Fig. 2a**). In addition to differences between GF or CONV mice
114 and *Turicibacter*-monocolonized animals, there were also alterations in host lipids that showed
115 some strain-dependency, with trending discrepancies in dicarboxylate and significant differences
116 in long chain saturated fatty acids (**Fig. 2a**) At the tissue level, two of the four *Turicibacter*
117 strains stimulated statistically significant increases in epididymal/gonadal white adipose tissue
118 (e/gWAT) mass in comparison to GF controls, and a third strain elicited similar increases that
119 were not statistically significant (T129). In contrast, there was no noticeable effect of H121 on
120 e/gWAT mass (**Fig. 2c, Supplementary Table 3**), distinguishing it from the other *Turicibacter*
121 strains. Consistent with this, H121 showed the smallest e/gWAT adipocyte size within fat pads
122 (**Supplementary Fig. 1a-f**). This may be due to lower colonization of H121 in both the small
123 intestine and the colon (**Supplementary Fig. 1g, h**) The effects of particular *Turicibacter* strains
124 on serum lipids, cholesterol, and fat mass directed us to investigate molecules that could
125 potentially connect these biomolecules: bile acids.

126 Bile acids can affect circulating host lipids by altering fat digestion and systemic
127 hormonal signaling[40]. They are produced by the host and released into the small intestine, where
128 they promote digestion of fats by facilitating micelle formation, and can also act through
129 receptors like the farnesoid X receptor (FXR)[40] and GPBAR1/TGR5[41]. Gut bacteria can modify
130 bile acids, primarily through transformations like deconjugation. Previous reports found that
131 MOL361 can broadly modify bile acids *in vitro*[21], so to determine if these abilities allowed
132 MOL361 and other *Turicibacter* strains to modify host bile acids *in vivo*, we profiled serum and
133 cecal bile acids in *Turicibacter*-monocolonized mice. Though each strain had some unique

134 impacts on host serum metabolites, we noted some consistent patterns in bile acids across
135 monocolonized mice in comparison to either their GF or CONV controls. (Note: bile species
136 with amino acid conjugants are typically referred to as "bile salts," but for simplicity, we will
137 herein refer to both conjugated and unconjugated bile species as "bile acids"). Colonization with
138 all of the *Turicibacter* strains led to a general increase in serum levels of unconjugated primary
139 bile acids like cholate (CA), chenodeoxycholate (CDCA), and β-muricholate (βMCA) (**Fig. 3a-**
140 **d**), and a similar rise in unconjugated secondary bile acids 3-dehydrocholate and 7-
141 ketodeoxycholate (**Fig. 3e,f**). These responses were highly variable in the case of T129
142 colonization, leading us to de-emphasize this strain for subsequent experiments. In response to
143 colonization with MOL361, 1E2, or H121, we also found a similar increase in several
144 unconjugated bile acids in the cecum (**Supplemental Fig. S2).** In all, these results suggest that
145 these *Turicibacter* strains are able to impact host bile acids, potentially by deconjugating them in
146 the gut.

147 When we investigated potential explanations for increases in unconjugated bile species,
148 we noticed that the serum levels of conjugated bile acids differed between animals colonized by
149 different *Turicibacter* strains, with the clearest delineation separating H121 from MOL361 and
150 1E2. MOL361- and 1E2-colonized animals generally had lower levels of taurine-conjugated
151 primary bile acids in comparison to H121-colonized animals (**Fig. 3g-j**), whereas H121
152 colonization led to an increase in glyco-beta-muricholic acid (GβMCA) (**Fig. 3k**). Female mice
153 displayed the most significant *Turicibacter*-associated changes in circulating bile species, lipids,
154 and cholesterol, indicating sex-dependent responses to *Turicibacter* colonization
155 (**Supplementary Fig. 3**). This sex difference has also been reported in C57BL/6 mice
156 monocolonized with *T. sanguinis* MOL361, albeit with a directionally different change in
157 adipocyte size[38]. Notably, in the cecum, there was less strain-specific distinction in conjugated
158 bile acids, with taurine-conjugated bile acids decreased by colonization with any of the three

159 *Turicibacter* strains we surveyed (**Supplementary Fig. S2**). The one cecal bile acid that did
160 display strain dependency was the secondary bile acid lithocholic acid (**Supplementary Fig. S2,**
161 **bottom**). Also, the low levels of detected glycine-conjugated bile acids (specifically glycocholic
162 acid) in both serum and cecal contents was slightly increased by *Turicibacter* colonization (**Fig.**
163 **3k,l; Supplementary Fig. S2c**) Overall, these data demonstrate that colonization with
164 *Turicibacter* alters serum bile acids, lipids, and cholesterol, as well as host fat mass. Further,
165 while some changes like increased unconjugated bile acids were conserved across *Turicibacter*
166 colonizations, levels of specific conjugated bile acids differed between *Turicibacter* strains, with
167 MOL361 and 1E2 leading to lower levels of taurine-conjugated bile acids than H121
168 colonization.
169
170 Turicibacter *strains differ in their ability to modify host bile acids*
171
172 Based on the large genetic variation between the *Turicibacter* strains (**Fig. 1**) and the
173 differences in aspects of serum lipid and bile acid profiles seen in response to colonization with
174 different strains (**Fig. 3**), we posited that these strains differ in their ability to modify bile acids.
175 To test this, we grew each of our nine isolates to stationary phase in rich medium supplemented
176 with a sub-inhibitory concentration of five bile species[21]: cholic acid, chenodeoxycholic acid,
177 deoxycholic acid (DCA), taurocholic acid (TCA) and glycochenodeoxycholic acid (GCDCA).
178 We then used liquid chromatography-mass spectrometry (LC-MS) to characterize the resulting
179 bile transformations performed by each isolate (**Fig. 4a**). We discovered that the strains not only
180 differed in their ability to modify this combination of bile species, but also that these capabilities
181 generally mirrored the groupings identified in genomic comparisons (**Fig. 4b**). MOL361, 18F6,
182 and GALT-E2 deconjugated both tauro- and glyco-bile acids, and also dehydrogenated CA and
183 CDCA (**Fig. 4b**). 1E2 and TA25 deconjugated tauro-bile acids, but did not detectably

184 deconjugate glyco-bile acids or perform dehydrogenation (**Fig. 4b**). H121 and T129
185 deconjugated glyco-bile acids, but did not readily deconjugate tauro-bile acids nor perform
186 detectable dehydrogenation (**Fig. 4b**). T46 and GALT-G1 did not have bile-modifying capacity
187 that mirrored their genetic phylogeny; T46 genomically resembled the MOL361 group but
188 performed modifications similar to the H121 group (*i.e.* glyco- but not tauro- deconjugation,
189 minimal dehydrogenation), whereas GALT-G1, which genomically resembled the H121 group,
190 performed more MOL361-like transformations (*i.e.* glyco- and tauro-deconjugation,
191 dehydrogenation of CDCA) (**Fig. 1, 4b, Supplementary Fig. 4**). Overall, each strain performed
192 at least one of three bile transformations, with some showing capacity for all three (**Fig. 4b,**
193 **Supplementary Fig. 4**).
194 To confirm these intragroup distinctions, we chose one isolate from each of the
195 subgroups (MOL361, H121, 1E2), and grew them in the presence of four primary conjugated
196 bile acids: TCA, taurochenodeoxycholic acid (TCDCA), glycocholic acid (GCA), and GCDCA.
197 This supported the same pattern seen above; MOL361 deconjugated both groups of bile acids,
198 1E2 preferentially deconjugated tauro-conjugates, and H121 preferentially deconjugated glyco-
199 conjugates (**Fig. 4c**). MOL361 and 1E2 displayed broad deconjugation of tauro-conjugates and
200 were able to process at least six taurine-conjugated bile acids (**Supplementary Fig. 5**). These
201 data reveal that while all tested strains are efficient modifiers of bile species, their specific
202 transformations differ in a strain-dependent manner, potentially reflecting functions that
203 influence their differential effects on host lipid biology.
204
205 Turicibacter *genomes have different repertoires of bile salt hydrolases*
206
207 The different bile modification abilities across strain subgroups suggested that each
208 contained unique repertoires of bile-modifying genes. Certain bacteria from the gut microbiota

209 dehydrogenate hydroxyl groups from the steroid core of bile acids[42], increasing their polarity and
210 modulating their affinity for host bile acid receptors[43]. We searched the *Turicibacter* genomes for
211 homologs of the characterized 7α-hydroxysteroid dehydrogenase (7α-HSDH[21]) from *Clostridium*
212 *absolum*[44]. This revealed genes with 57% amino acid identity in MOL361, 18F6, T46, and
213 GALT-E2, and homologs with 59% amino acid identity in H121 and T129 (**Supplementary Fig.**
214 **6a**). Though the H121-derived putative homolog had higher overall sequence identity than the
215 MOL361-derived homolog, it lacked certain features predicted to be critical for dehydrogenase
216 activity, such as the analogous Asp38 that is catalytically critical for this reaction[44]. Because *in*
217 *vitro* experiments showed only isolates from the MOL361 group performed bile
218 dehydrogenation, we cloned the putative 7α-HSDH homolog from MOL361 into *E. coli* C41-
219 pLys and then grew these cells in individual unconjugated bile acids that can be dehydrogenated:
220 CA, CDCA, and DCA. Indeed, the protein encoded by the gene removed the mass equivalent of
221 two hydrogens from CA (**Supplementary Fig. 6b, c**). Background transformation by *E. coli*
222 prevented clear evidence of CDCA dehydrogenation by this putative 7α-HSDH homolog
223 (**Supplementary Fig. 6d**), but this homolog did not act on DCA (**Supplementary Fig. 6e**),
224 supporting its annotation as a 7α-HSDH.
225 Conjugation increases bile acid solubility and emulsification ability[45], while
226 deconjugation reverses these effects, leading to decreased dietary lipid absorption. To identify
227 *Turicibacter* bile salt hydrolase (*bsh*) genes responsible for the strain-specific differences in bile
228 deconjugation, we first searched our assembled genomes for annotations of "choloylglycine
229 hydrolase," the broad category that includes these genes. Of these annotated genes, we identified
230 eight groups of potentially homologous sequences, and found that each *Turicibacter* strain
231 encodes putative choloylglycine hydrolases from at least two of the eight groups **(Fig. 5a, b**).
232 Isolates within the same phylogenetic and phenotypic subgroups largely shared similar
233 sequences (**Fig. 5a, b**). To assay the function of the strain-specific putative *bsh* genes, we cloned

234 and individually expressed one representative sequence from each of the eight putative
235 choloylglycine hydrolase groups in *E. coli* C41-pLys and measured the ability of these
236 engineered bacteria to perform the deconjugations we observed in our native *Turicibacter*. We
237 cultured the individual *E. coli* strains to stationary phase in the presence of two tauro- (TCA,
238 TCDCA) or glyco- (GCA, GCDCA) bile acids, then measured their ability to deconjugate these
239 bile acid pools. We found that *E. coli* expressing four of the eight putative *bsh* gene groups
240 showed deconjugation activity against at least one of the bile acids (**Fig. 5c-e**). From MOL361,
241 one BSH (group IV) is tauro-specific, and one (group I) deconjugates both glyco- and tauro-
242 conjugates (**Fig. 5c, d**). 1E2 shares a tauro-specific BSH with MOL361 (group IV), and has
243 another BSH (group III) with moderate activity on TCDCA (**Fig. 5c, d**). H121 has a BSH (group
244 II) with activity on TCDCA and GCDCA (**Fig. 5c, d**), although this was blunted when presented
245 with the combined four bile acids (**Fig. 5e**), potentially because of competitive inhibition.
246 Collectively, these findings reveal that *Turicibacter* strains contain a range of bile salt hydrolases
247 with deconjugation preferences for different bile acids.
248
249 *Strain- and substrate-specific bile salt hydrolases from* Turicibacter *differentially alter host lipid*
250 *composition*
251
252 Given that *Turicibacter* colonization broadly modified host lipid and bile pools (**Fig. 2**),
253 and that bile transformations have been previously shown to alter host lipids[46,47], we predicted
254 that expressing *Turicibacter* bile-modifying genes outside the context of *Turicibacter*
255 colonization would be sufficient to impact host lipid biology. To measure the individual effects
256 of these bile acid transformations, we expressed *Turicibacter bsh* genes off of a genomically-
257 integrated high expression vector[48] in the common gut bacterium *Bacteroides thetaiotaomicron*.
258 This bacterium was chosen because it stably colonizes the murine gut and, unlike *E. coli* C41-

259 pLys, contains a homolog of a characterized 7α-HSDH similar to that of *T. sanguinis*
260 MOL361[49,50], allowing the engineered bacteria to more completely mimic *Turicibacter* bile
261 transformations. As this *B. thetaiotaomicron* strain has previously been described to have some
262 BSH activity[46], we decided to employ the parental strain expressing the non-bile modifying
263 green fluorescent protein (GFP) as a comparison baseline for these experiments (named *Bt*-WT).
264 These engineered *B. thetaiotaomicron* strains generally transformed tauro- and glyco- conjugated
265 bile acids as predicted based on the BSH characterization in *E. coli*, including preferential
266 TCDCA transformation, indicating they were capable of performing *Turicibacter*-like bile
267 transformations (**Fig. 6a, Supplementary Fig. 7**). However, the *B. thetaiotaomicron* strain that
268 expressed *bsh* (group III) from strain 1E2 more completely transformed glyco-conjugated bile
269 acids than the strain expressing *bsh* (group II) from H121, counter to the *E. coli* findings. This
270 observation led us to not use the *bsh* (group II)-expressing strain further. Additionally, although
271 we did not notice a significant *in vitro* growth defect in the engineered *B. thetaiotaomicron*
272 strains (**Supplementary Fig. 8)**, we observed a bile transformation delay in *B. thetaiotaomicron*
273 expressing *bsh* (group I) from MOL361 that we could compensate for by extending the growth
274 period (**Fig. 6b**).

275 We monocolonized mice with the *bsh*-expressing *B. thetaiotaomicron* strains and
276 assessed their circulating lipid profiles and abdominal WAT mass. We found that the engineered
277 strains colonized the gnotobiotic mouse gut at least as well as the parental strain, with one strain
278 (BSH-III-1E2) colonizing the cecum slightly better (**Supplemental Fig. 9**), and that expressing
279 individual *Turicibacter bsh* genes in the *B. thetaiotaomicron* background was sufficient to
280 significantly alter host cecal bile levels (**Fig. 6c, Supplementary Fig. S10**) and the absolute
281 abundance of hundreds of circulating lipid species (**Fig. 6d, Supplementary Table 4**). In
282 particular, expression of either the group I or group IV *bsh* led to a decrease in triglycerides (**Fig.
283 6d, e**). Expressing the tauro-specific *bsh* (group IV) from MOL361 also decreased

284 diacylglycerides (**Fig. 6g**). Expressing the broader specificity *bsh* (group I) from MOL361 also
285 led to a decrease of phosphatidylglycines, phosphatidylserines, and cholesterol (**Fig. 6d-f, h, i**).
286 Despite having broad capacity for transformation, *B. thetaiotaomicron* expressing *bsh* (group III)
287 from 1E2 did not alter host lipid profiles as much as the other strains **(Fig. 6d-i**). On a tissue-
288 level, *bsh*-expression also altered WAT storage in the colonized mice, with the broad tauro-
289 deconjugating BSHs (group I and IV) significantly reducing WAT mass (**Fig. 6j**). Similar to our
290 findings with *Turicibacter* monocolonization, we also observed a sex difference in BSH
291 responses, with male mice showing more consistent decrease in triglycerides in response to the
292 tauro-specific BSH from MOL361, and females showing more consistent triglyceride responses
293 to the broadly deconjugating BSH (**Supplementary Fig. 12**). Overall, these BSH-associated
294 lipid and adipose tissues results were consistent with previous findings on MOL361 colonization
295 in the C57Bl/6 mouse model[38], but differed from MOL361 colonization in our Swiss Webster
296 mice (**Fig. 2c, Supplementary Fig. S13**).

297 To further explore potential factors that may drive the cholesterol and WAT alterations in
298 response to *Turicibacter* colonization and *bsh* expression, we measured liver transcript levels of
299 farnesoid X receptor, (Fxr), a key nuclear receptor for bile acids; cytochrome P450 Family A
300 Subfamily A Member 1/Cholesterol 7α Hydroxylase (Cyp7a1), the rate-limiting enzyme for
301 conversion of cholesterol into bile acids; and glucose-6-phosphatase (G6pase), a key enzyme for
302 gluconeogenesis. There were no differences in Fxr transcript levels across any of the native and
303 engineered bacterial colonization conditions (**Supplementary Fig. 14a**). However, we found
304 similar increases in Cyp7a1 expression (**Supplementary Fig. 14b**) and decreases in G6pase
305 expression (**Supplementary Fig. 14c**) between the *Turicibacter* and *bsh* colonizations. These
306 findings suggest that the bile-modifying activities of *Turicibacter* lead to downstream alterations
307 in liver expression of bile signaling and response elements. In all, these results demonstrate that
308 expressing strain-specific *bsh* genes from *Turicibacter*, especially those able to process the

309 abundant taurine-conjugated bile acids present in the murine intestine, is sufficient to alter host
310 cholesterol, bile, and lipid biology.
311
312 ***Discussion***
313
314 Results from this study show that several strains of *Turicibacter* bacteria from the
315 mammalian gut microbiota modulate host bile and lipid compositions. We identified and
316 characterized five novel *Turicibacter* genes capable of performing bile transformations (four *bsh*,
317 one 7α-HSDH), and revealed that expression of individual *bsh* genes is sufficient to broadly and
318 differentially alter host lipid profiles. Further, we found that while bile-transforming genes are
319 present in all our surveyed *Turicibacter* strains, the specific transformation capacity of BSH
320 variants differed by strain in a manner consistent with host environment co-evolution: bile acids
321 in the human gut are a mix of taurine- and glycine-conjugants, whereas murine bile acids are
322 predominantly taurine-conjugants[51,52], providing different bile environments that are
323 preferentially processed by *Turicibacter* strains isolated from their respective gastrointestinal
324 tracts. This close connection between host-specific bile composition and bacterial modifications
325 may be due in part to the bile sensitivity previously exhibited by MOL361 and/or the high
326 abundance of *Turicibacter* in the small intestine, causing these bacteria to more strongly
327 associate with host genes for bile reabsorption and lumenal bile levels than other bile-modifying
328 gut bacteria[21,53–57].
329 This work displays metabolic consequences of colonization by specific gut bacteria and
330 improves the resolution of our understanding connecting specific taxa—in this case, at the strain
331 level—with host physiology. In rodent and human studies, *Turicibacter* relative abundance often
332 negatively correlates with dietary fats[29,31,58–62] and host adiposity[28,33,63], but some studies have
333 shown opposite relationships[30,64,65]. This could be a result of the phenotypic diversity identified

334 here among *Turicibacter* isolates wherein the host may experience different lipid outcomes
335 depending on their own specific *Turicibacter* strains, but could also vary with other features such
336 as host genetics and sex[21,38] (**Supplementary Fig. 3, 11, 12**), leading to discrepancies in lipid
337 responses between hosts despite similar bile modifications performed in the gut microbiota.
338 Importantly, effects of *Turicibacter* colonization could also be influenced by biogeographic
339 organization of an individual's microbiota; in addition to the specific taxonomic membership,
340 *Turicibacter* positioning in the small and large intestine may affect host consequences from their
341 respective bile modifications by transforming bile pools in either section of the gut tract. Despite
342 genomic and localization differences between them, we found that MOL361 and H121 induced
343 lipid metabolite changes that indicate increases in fatty acid oxidation, suggesting that these
344 strains at least share features that alter host fatty acid metabolism. While we identified some host
345 lipids that were differentially modulated by different *Turicibacter* strains, host complexities
346 likely reduced our power to further resolve these differences, pointing to future research that may
347 still reveal more strain-specific effects of *Turicibacter* bacteria.

348 Further research into *bsh* gene regulation in the *Turicibacter* genus, the relationship
349 between bile and *Turicibacter* colonization and transmission behaviors, as well as the native
350 functionality of the putative BSH and 7α-HSDH homologs we tested, will further explain how
351 these bacteria wield their bile modifications in the intestine. In addition, exploring the
352 discrepencies we observed between bacterially-induced serum and cecal bile profiles could
353 describe other complexities in these effects, such as differential host reabsorption of modified
354 bile acids. Several of the *in vitro* bile modulations, such as increases in unconjugated bile acids,
355 were consistent between our *in vitro* characterizations and *Turicibacter* colonization, but
356 concurrent *in vivo* increases in expression of bile synthesis genes and levels of glyco-conjugated
357 bile acids seen during *Turicibacter* colonization and expression of individual *Turicibacter* BSH
358 indicate the possibility of more complex interactions between host bile production and

359 *Turicibacter* activity. The fact that the specificity and activity of the individual BSH homologs
360 differed when expressed in different bacterial backgrounds indicates that other unknown cellular
361 or environmental factors influence the way individual BSH act *in vivo.* This may also include
362 mechanisms that modify the functionality of the other putative BSH homologs we identified
363 from *Turicibacter* that did not deconjugate the specific conjugated bile acids used in our
364 experiments. These findings may influence the ways that bile-modifying genes can be employed
365 to shape host lipid profiles through microbiota engineering, positioning certain microbial species
366 as more appropriate vectors to impart specific host effects. It will also be informative to
367 determine what other activities performed by *Turicibacter* lead to WAT gain in colonized
368 animals, which contrasted findings from colonizing mice with specific *bsh*-overexpressing
369 strains of *B. thetaiotaomicron*. Given this finding, it is likely that *Turicibacter* also influences
370 host lipids through other mechanisms in addition to the bile transformations we characterized.

371 Our work also connects specific *Turicibacter* members and BSH activity with specific
372 host outcomes. Though some host responses such as broadly decreased triglycerides were
373 consistent across our BSH-recipient mice, the exact lipid and cholesterol responses differed,
374 indicating that the type of deconjugations might have differing connections with host physiology.
375 Further work will continue strengthening the exciting prospect of utilizing *Turicibacter* and/or its
376 bile modifications to intentionally alter host lipid biology to improve host metabolic and lipid-
377 associated health[66,67], as has been proposed with other bacteria[54,68]. Beyond lipid biology,
378 *Turicibacter* abundance has been positively correlated with diseases such as Parkinson's
379 disease[69] and depression[70], and selective serotonin reuptake inhibitors (SSRIs) have been found
380 to negatively affect *Turicibacter* growth and colonization[71], potentially because they inhibit
381 activity of its unique serotonin transporter[38]. SSRI use is frequently associated with metabolic
382 side effects like weight gain[72,73], and our findings suggests a hypothesis that connects SSRI use
383 and these side effects: SSRI use could diminish gut colonization of bacteria like *Turicibacter*,

384 thus unintentionally altering their impact on host physiology. Future work may develop
385 strategies to reduce interactions between SSRIs and activity of the microbiota, and minimizing
386 the side effects of these drugs and improving host outcomes. In all, these associations further
387 emphasize the importance of understanding mechanisms connecting members of the diverse
388 *Turicibacter* genus to host physiology.
389
390
391 ***Methods***
392
393 *Mouse husbandry*
394 Adult (6-8 week old) germ-free Swiss Webster mice were used for all animal
395 experiments according to UCLA Institutional Animal Care and Use Committee-approved
396 protocols. Mice were reared in flexible gnotobiotic isolators on a 12h:12h light dark schedule on
397 standard chow (Labdiet 5K52, 22.1%: 16.6%: 61.3% protein: fat: carbohydrate by calories), then
398 were exited to autoclaved filter top cages with autoclaved chow (Labdiet 5010, 28.7%: 13.1%:
399 58.2% protein: fat: carbohydrate by calories) and water. After one day of cage acclimation, the
400 noted *Turicibacter* or *Bacteroides thetaiotaomicron* strain was grown in YCFA medium (see
401 below) overnight, pelleted by centrifugation, and resuspended in 1X PBS. Mice were colonized
402 by a 200μL gavage containing ~10^6 colony-forming units (CFU) of *Turicibacter* or ~10^8 CFU of
403 *B. thetaiotaomicron*. Alternatively, mice were gavaged with the same volume of PBS alone
404 (referred to as germ-free [GF]) or PBS-suspended fecal slurry from a specific pathogen-free
405 adult mouse (referred to as conventionalized [CONV]). Colonization was quantified using strain-
406 specific TuriSERT primers (**Supplementary Table 5)** and quantitative PCR (qPCR) from
407 weight-normalized contents from the distal small intestine and proximal colon after addition of
408 Low Abundance Microbiota Standard (Zymo) and extraction using the Zymo DNA Mini kit

409 (Zymo), standardized to a standard curve of CFU derived from plating of serial dilutions from
410 cultures of that strain.
411
412 *Bacterial culturing*
413 *Turicibacter* isolates and *Bacteroides thetaiotaomicron* strains (**Supplementary Table 1**)
414 were cultured in a flexible vinyl chamber (Coy) in an anaerobic 85%/10%/5% nitrogen/carbon
415 dioxide/hydrogen mixture (Airgas). *Turicibacter* was grown on Schaedler's agar (BD
416 Biosciences) or modified YCFA[74] (pH 7.4, per liter: 100mM MOPS, 10g casitone, 2.5g yeast
417 extract, 2g glucose, 2g maltose monohydrate, 2g cellobiose, 44mg $MgSO_4$, 68mg $CaCl_2$, 0.9g
418 NaCl, 10mg hemin, 0.45g K_2HPO_4, 0.45g KH_2PO_4, 4g $NaHCO_3$, 1g cysteine, 1mg resazurin,
419 1.9mL glacial acetic acid, 0.7mL propionic acid, 90μL isobutyric acid, 100uL isovaleric acid,
420 100uL valeric acid, 10mL ATCC vitamin mixture, 0.2% Tween-80) at 37°C. Cells were normally
421 grown without shaking, but when appropriate, *Turicibacter* cultures were anaerobically
422 transferred to sealed Hungate tubes or 1.7mL microcentrifuge tubes and shaken at 225 RPM at
423 37°C.
424 For *B. thetaiotaomicron* growth curves, overnight cultures were grown anaerobically in
425 BHI-S for ~48 hours at 37 ^{o}C to ensure culture saturation, then were subcultured 1:50 for 6 hours
426 at 37 ^{o}C (final OD_{600}=0.41-0.51). Subcultures were all then diluted to OD_{600}=0.1, and then six
427 replicates were further diluted 1:10 in 100μL BHI-S in a 96 well plate. Plates were anaerobically
428 sealed with parafilm and incubated at 37 ^{o}C. OD_{600} readings were taken every 15 minutes in a
429 Biotek Synergy H1 microplate reader (Agilent).
430 *Escherichia coli* C41-pLys (Lucigen) was used for characterizing putative bile
431 modification genes, which were expressed off the pET21+ plasmid. *E. coli* was grown
432 aerobically shaking at 37°C C in Luria Broth (LB, 1% NaCl, 1% tryptone, 0.5% yeast extract)

433 supplemented with 100μg mL^{-1} ampicillin. Expression of genes was induced by addition of
434 100μM IPTG.
435
436 *Bacterial isolation and identification*
437 The frozen stool sample was thawed on ice and diluted 1:10 with PRAS anaerobic
438 dilution blank medium (Anaerobe Systems). 100μL of the diluted stool was further diluted to
439 1:1000 with modified YCFA media containing 0.05% bovine bile, 0.2% Tween-80, and 50mM
440 resorufin and loaded on Prospector® system arrays (Isolation Bio, San Carlos, CA, USA)
441 following manufacturer's instructions. The fluorescent green signal of the arrays at time 0 was
442 read on the Prospector® instrument in a Coy anaerobic chamber and the arrays incubated at 37°C
443 in an Anaerobic Systems AS-580 anaerobic chamber (Anaerobe Systems). At 17 and 41 hours of
444 incubation the arrays were scanned again and the decrease in green fluorescence from time 0 was
445 used as an indicator for bacterial growth in the array nanowells. Bacteria from the array were
446 transferred to 96-well transfer plates containing 200μL per well of modified YCFA media,
447 without the addition of 50mM resorufin. The transfer plates were sealed with a gas permeable
448 film and incubated at 37°C in a Mitsubishi AnaeroPack jar with a gas-generating sachet (Remel)
449 for seven days. After incubation, the contents of 538 wells from the transfer plates with visible
450 turbidity were consolidated into secondary 96-well plates, preserved with reduced glycerol, and
451 stored at -80°C until needed. Unless stated otherwise, all stool and isolate manipulations were
452 conducted anaerobically with a 5% CO_2/5% H_2/90% N_2 atmosphere.
453 Genomic DNA was extracted in a 96-well format from the consolidated Prospector®
454 culture plates using the Extract All Kit (Applied Biosystems). 20μL of culture was combined
455 with 20μL of Lysis Solution and incubated for 10 minutes at 95°C, followed by three minutes at
456 room temperature. The DNA was stabilized with the addition of 20μL of DNA Stabilizing
457 Solution and the resulting DNA lysate stored at -20°C until needed.

458

459 *qPCR screening of novel* Turicibacter *isolates*

460 Genomic DNA from 538 isolates was screened for *Turicibacter* 16S and the *Turicibacter*
461 TuriSERT[38] gene using a multiplexed primer set (**Supplementary Table 5**). Each 25µL qPCR
462 reaction mixture had 1µL Extract All lysate, 10µL SYBR Power master mix (Applied
463 Biosystems), 0.5µL of each of the 10µM primers, and 12µL molecular grade water. The reactions
464 were run in a QuantStudio 6 Flex (Thermo Fisher) with a 95°C hold followed by 40 cycles of
465 95°C for 15s, 50°C for 30s, 72°C for 30s. *Turicibacter sanguinis* MOL361 gDNA and water were
466 used as positive and negative controls, respectively.

467

468 *Molecular cloning*

469 *Turicibacter* genes were amplified from template culture lysates with Phusion or Q5
470 DNA polymerase (NEB) and primers designed to amplify denoted *Turicibacter* genes. pET21- or
471 pWW3837[48]-derived expression plasmids were assembled using Gibson assembly (see
472 **Supplementary Table 5** for oligos) for expression in *E. coli* or *Bacteroides thetaiotaomicron*,
473 respectively. Cloned constructs were confirmed through Sanger sequencing prior to functional
474 characterization. pWW3837-derived constructs were cloned into *B. thetaiotaomicron* VPI-5482
475 as previously described[48,75]. *bsh*-expressing *B. thetaiotaomicron* was compared to *B.*
476 *thetaiotaomicron* containing the original pWW3837 construct (referred to as wild-type *B.*
477 *thetaiotaomicron*).

478

479 *Genome assemblies*

480 Each strain was streaked on Schaedler agar plates and incubated anaerobically, then an
481 individual colony from each isolate was picked into YCFA medium and grown overnight at
482 37°C. DNA was extracted using the Zymo DNA mini kit (Zymo), with bead beating used to lyse

483 cells. Purified genomic DNA was sequenced by MiGS (migscenter.org), and 151bp paired-end
484 sequences were assembled using CLC Genomics Workbench (Qiagen). Genome assemblies have
485 been deposited at NCBI at BioProject PRJNA846348.
486
487 *Whole genome and gene comparisons*
488 anvi'o[76] was used to profile and visualize the different *Turicibacter* strain DNA
489 sequences to locate putative bile salt hydrolase and 7α-HSDH homologs in contig groups,
490 generate variability profiles, and measure gene coverage and detection statistics. Average
491 nucleotide identity (ANI) was calculated using OrthoANIu[77] (available
492 https://www.ezbiocloud.net/tools/ani).
493 Sequences comparisons between 16S rRNA and *bsh* genes/BSH amino acid sequences
494 were performed in CLC Genomics Workbench (Qiagen). 7α-HSDH sequence comparisons were
495 performed using tblastn[78] using the translated amino acid sequence from *Clostridium absonum*[44].
496
497 *Assessment of bile transformations*
498 *In vitro* characterization of bile transformations by engineered *E. coli* or *B.*
499 *thetaiotaomicron* strains were performed by growing cells in respective media conditions
500 described above supplemented with 0.5mM (total combined concentration) of the noted bile
501 species. Cells were grown to stationary phase (shaking at 37°C), then frozen at -80°C until
502 further processing. Cells were then thawed, pelleted (5 minutes at 16,000 x g), and the
503 supernatant was removed to a new microcentrifuge tube. Three volumes of methanol was added,
504 then the mixture was vigorously mixed for 30-60 seconds and incubated (room temperature, 15
505 minutes). Mixtures were centrifuged (5 minutes, 16,000 x g), the supernatant removed to a clean
506 microcentrifuge tube and dried in a vacuum concentrator. The dried residue was treated with
507 methanol/water/formic acid (50/50/0.1, all by volume) then vigorously mixed and centrifuged as

508 described above. Supernatants were transferred to polypropylene HPLC vials, capped, and
509 maintained at 4°C while aliquots (typically 5μL) were injected onto a reversed phase HPLC
510 column (Cadenza CD-C18, 3.0μm, 250 x 2mm, Imtakt) equilibrated in solution A (water/formic
511 acid, 100/0.1, vol./vol.) and eluted (0.2mL minute^{-1}) with an increasing concentration of solution
512 B (acetonitrile/formic acid, 100/0.1, vol./vol.); minute/% B: 0/30, 45/70, 48/100, 50/30, 67/30).
513 The effluent from the column was passed through an electrospray ion source (capillary voltage
514 42V, capillary temperature 275°C, sheath gas flow 15L min^{-1}, spray voltage 5kV, and -15kV
515 conversion dynode with -1.2kV multipliers) connected to a linear ion trap mass spectrometer
516 (Thermo LTQ) scanning from m/z 95-1000 in the positive ion mode. Spectra were recorded and
517 analyzed with instrument-manufacturer supplied software. Confirmation of proposed elemental
518 compositions was achieved using the same chromatography and ion source configuration with
519 the spectra recorded by scanning on an orbitrap mass spectrometer (Thermo LTQ XL).
520 For bile species quantification, an internal spike-in standard of 100mM chenodeoxycholic
521 acid-D4 (CDCA-D4, Sigma) was added to initial culture supernatants as a normalization
522 reference. Area under the curve from reconstructed ion chromatograms was used to quantify the
523 abundances of each species.
524
525 *Serum metabolite analysis*
526 Mice were euthanized with isoflurane and whole blood was collected via cardiac
527 puncture. Blood was allowed to clot in SST Vacutainer tubes (BD) on ice, then centrifuged (4°C,
528 1 minute, 1500 x g). The supernatant was removed and snap frozen in liquid nitrogen. Serum
529 metabolites were analyzed using global metabolomics platform by Metabolon (Morrisville, NC,
530 USA). Unless otherwise noted, values presented are in arbitrary units (a.u.) for that particular
531 metabolite, determined by the log-transform of the volume-corrected quantification.
532

533 *Circulating lipid analysis*

534 Mice were fasted for 4-6 hours, then euthanized as described above. Blood was collected
535 via cardiac puncture and deposited into anticoagulatory K_2EDTA Vacutainer tubes (BD) on ice.
536 Blood was centrifuged (4^oC, 15 minutes, 2000 x g), then plasma was collected from supernatant
537 and snap frozen in liquid nitrogen. Shotgun lipidomics was performed by the UCLA Lipidomics
538 Core (Los Angeles, CA, USA) with the following protocol. Thawed plasma was pipetted into
539 glass tubes, a mixture of 70 internal standard lipids (Sciex and Avanti) was added, and lipids
540 were extracted using a modified Bligh and Dyer extraction[79]. The pooled organic layers from
541 two extractions were dried in a vacuum concentrator and resuspended in 50/50 (vol./vol.)
542 methanol/dichloromethane plus 10mM ammonium acetate. After transfer to robovials, samples
543 were analyzed with a Sciex 5500 with DMS Device (Lipidyzer Platform) using a targeted
544 acquisition list of 1450 lipid species. The Lipidyzer Differential Mobility device was tuned using
545 the EquiSPLASH LIPIDOMIX standard mixture (Avanti). Data was analyzed using an in-house
546 platform using previously described parameters[80], and quantitative values were normalized to
547 input volume. Statistical significance identification for species to include in heatmap was
548 performed with uncorrected two-tailed Welch's t-test comparison to Bt-WT (p-value cutoff
549 <0.05). Both raw and corrected p-values are included in Supplementary Table 4.

550

551 *Total cecal bile analysis*

552 Mice were colonized as described above and contents from the blind end of the cecum
553 were snap frozen upon sacrifice. Samples were thawed on ice and sent to Metabolon for analysis
554 with total bile analysis pipeline. Values shown at "0" were non-quantified and below limit of
555 detection.

556

557 *Adipocyte area calculation*

558 After sacrifice, mice epidydimal or gonadal white adipose tissue (e/g WAT) pads were
559 weighed and placed into 4% paraformaldehyde in 1X PBS for 48 hours at 4°C. Fat pads were
560 washed twice in 70% ethanol, then submitted to the UCLA Translational Pathology Core
561 Laboratory (Los Angeles, CA, USA) for paraffin embedding, sectioning, and H&E staining. Ten
562 adipocyte images from each animal (five from each fat pad) were visualized with a 20X
563 objective on an EVOS microscope (Thermo). Adipocyte area for all cells contained entirely
564 within the field of view was automatically measured using the Fiji[81] Adiposoft[82] plug-in (version
565 1.1.16).
566
567 *qRT-PCR measurement of liver transcripts*
568 Gnotobiotic mice were colonized with single bacterial strains as described above, and
569 upon sacrifice, the median lobe of the liver was dissected and either directly snap frozen in liquid
570 nitrogen (all *Turicibacter* colonized animals) or placed in Trizol, bead beat for one minute, then
571 frozen in liquid nitrogen (all *B. thetaiotaomicron* colonized animals). All livers were then
572 transferred to -80°C until further processing. Directly snap frozen livers were thawed overnight
573 at -20°C in RNALater-ICE (ThermoFisher), then bead beat in Trizol for one minute, after which
574 all samples were processed in the same manner. RNA was extracted from thawed Trizol samples
575 using the Direct-Zol RNA Miniprep Kit (Zymo), then cDNA was generated using the qScript
576 cDNA Synthesis Kit (Quantabio). qPCR was performed using the PowerUp SYBR Green Master
577 Mix (ThermoFisher) on a QuantStudio5 Real-Time PCR System (ThermoFisher) (primers[83,84]
578 available in **Supplementary Table 5**) (cycling conditions: 50°C for 2 min, 95°C for 2 min, 50
579 cycles of 95°C for 15 sec, 55°C for 15 sec, 72°C for 1 min, followed by melt curve). Fold
580 changes in comparison with sex-matched controls (GF for *Turicibacter* colonizations, *Bt*-WT for
581 *B. thetaiotaomicron* colonizations) were calculated using the ΔΔCt method with auto-
582 thresholded Ct values with *ppia* as the housekeeping gene.

583

584 *Statistical analysis*

585 Statistical calculations were performed in in Prism 9.3.1 (Graphpad) or Microsoft Excel
586 14.7.1. When appropriate, outliers were detected using the ROUT method with Q=1% threshold
587 and removed from analysis. Dotted lines denote statistical comparison between groups directly
588 below line, solid lines denote pairwise comparison. Unless otherwise noted, all tests were two-
589 sided, *** = $p<0.0005$, ** = $p<0.005$, * = $p<0.05$, written p-value = $0.05 < 0.15$. Heatmaps were
590 created using the *pheatmap*[85] package in R (version 3.6.3)[86].

591

592

593 ***Data availability***

594 Metabolomics and lipidomics datasets are attached to this manuscript as supplementary tables.
595 Raw sequencing reads and genome assemblies for *Turicibacter* strains are deposited at NCBI
596 under BioProject ID PRJNA846348.

597

598 **REFERENCES**

599 1. Schoeler, M. & Caesar, R. Dietary lipids, gut microbiota and lipid metabolism. *Rev.*
600 *Endocr. Metab. Disord.* **20**, 461–472 (2019).
601 2. Wahlström, A., Sayin, S. I., Marschall, H.-U. & Bäckhed, F. Intestinal Crosstalk between
602 Bile Acids and Microbiota and Its Impact on Host Metabolism. *Cell Metab.* **24**, 41–50
603 (2016).
604 3. Sharon, G., Sampson, T. R., Geschwind, D. H. & Mazmanian, S. K. The Central Nervous
605 System and the Gut Microbiome. *Cell* (2016). doi:10.1016/j.cell.2016.10.027
606 4. Fung, T. C., Olson, C. A. & Hsiao, E. Y. Interactions between the microbiota, immune
607 and nervous systems in health and disease. *Nature Neuroscience* (2017).
608 doi:10.1038/nn.4476
609 5. Rabot, S. *et al.* Germ-free C57BL/6J mice are resistant to high-fat-diet-induced insulin
610 resistance and have altered cholesterol metabolism. *FASEB J.* **24**, 4948–4959 (2010).
611 6. Wikoff, W. R. *et al.* Metabolomics analysis reveals large effects of gut microflora on
612 mammalian blood metabolites. *Proc. Natl. Acad. Sci.* **106**, 3698–3703 (2009).
613 7. Yano, J. M. *et al.* Indigenous bacteria from the gut microbiota regulate host serotonin
614 biosynthesis. *Cell* (2015). doi:10.1016/j.cell.2015.02.047
615 8. Ivanov, I. I. *et al.* Induction of Intestinal Th17 Cells by Segmented Filamentous Bacteria.
616 *Cell* **139**, 485–498 (2009).
617 9. Sokol, H. *et al.* Faecalibacterium prausnitzii is an anti-inflammatory commensal
618 bacterium identified by gut microbiota analysis of Crohn disease patients. *Proc. Natl.*
619 *Acad. Sci.* **105**, 16731–16736 (2008).
620 10. Storelli, G. *et al.* Drosophila Perpetuates Nutritional Mutualism by Promoting the Fitness
621 of Its Intestinal Symbiont Lactobacillus plantarum. *Cell Metab.* **27**, 362-377.e8 (2018).
622 11. Kim, C. Y. *et al.* Human reference gut microbiome catalog including newly assembled

623 genomes from under-represented Asian metagenomes. *Genome Med.* **13**, 134 (2021).
624 12. Huang, S. *et al.* The day-to-day stability of the ruminal and fecal microbiota in lactating
625 dairy cows. *Microbiologyopen* **9**, (2020).
626 13. Maki, J. J. & Looft, T. Turicibacter bilis sp. nov., a novel bacterium isolated from the
627 chicken eggshell and swine ileum. *Int. J. Syst. Evol. Microbiol.* **72**, (2022).
628 14. Feng, Y. *et al.* Metagenome-assembled genomes and gene catalog from the chicken gut
629 microbiome aid in deciphering antibiotic resistomes. *Commun. Biol.* **4**, 1305 (2021).
630 15. Mo, J. *et al.* Structural and quantitative alterations of gut microbiota in experimental small
631 bowel obstruction. *PLoS One* **16**, e0255651 (2021).
632 16. Browne, H. P. *et al.* Culturing of 'unculturable' human microbiota reveals novel taxa and
633 extensive sporulation. *Nature* (2016). doi:10.1038/nature17645
634 17. Martínez, I. *et al.* The Gut Microbiota of Rural Papua New Guineans: Composition,
635 Diversity Patterns, and Ecological Processes. *Cell Rep.* **11**, 527–538 (2015).
636 18. Goodrich, J. K. *et al.* Genetic Determinants of the Gut Microbiome in UK Twins. *Cell*
637 *Host Microbe* **19**, 731–743 (2016).
638 19. Benson, A. K. *et al.* Individuality in gut microbiota composition is a complex polygenic
639 trait shaped by multiple environmental and host genetic factors. *Proc. Natl. Acad. Sci.*
640 **107**, 18933–18938 (2010).
641 20. Org, E. *et al.* Genetic and environmental control of host-gut microbiota interactions.
642 *Genome Res.* (2015). doi:10.1101/gr.194118.115
643 21. Kemis, J. H. *et al.* Genetic determinants of gut microbiota composition and bile acid
644 profiles in mice. *PLoS Genet.* (2019). doi:10.1371/journal.pgen.1008073
645 22. Santiago-Rodriguez, T. M. *et al.* Gut Microbiome of an 11th Century A.D. Pre-Columbian
646 Andean Mummy. *PLoS One* **10**, e0138135 (2015).
647 23. Wibowo, M. C. *et al.* Reconstruction of ancient microbial genomes from the human gut.

648 *Nature* **594**, 234–239 (2021).
649 24. Yatsunenko, T. *et al.* Human gut microbiome viewed across age and geography. *Nature*
650 **486**, 222–227 (2012).
651 25. Turnbaugh, P. J. *et al.* An obesity-associated gut microbiome with increased capacity for
652 energy harvest. *Nature* (2006). doi:10.1038/nature05414
653 26. Thaiss, C. A. *et al.* Persistent microbiome alterations modulate the rate of post-dieting
654 weight regain. *Nature* (2016). doi:10.1038/nature20796
655 27. Chadaideh, K. S. & Carmody, R. N. Host-microbial interactions in the metabolism of
656 different dietary fats. *Cell Metab.* **33**, 857–872 (2021).
657 28. Dhakal, S., McCormack, L. & Dey, M. Association of the Gut Microbiota with Weight-
658 Loss Response within a Retail Weight-Management Program. *Microorganisms* **8**, 1246
659 (2020).
660 29. Liu, W. *et al.* Diet- and Genetically-induced Obesity Produces Alterations in the
661 Microbiome, Inflammation and Wnt Pathway in the Intestine of Apc +/1638N Mice:
662 Comparisons and Contrasts. *J. Cancer* **7**, 1780–1790 (2016).
663 30. Li, T.-T. *et al.* Polyunsaturated fatty acids from microalgae Spirulina platensis modulates
664 lipid metabolism disorders and gut microbiota in high-fat diet rats. *Food Chem. Toxicol.*
665 **131**, 110558 (2019).
666 31. Velázquez, K. T. *et al.* Prolonged high-fat-diet feeding promotes non-alcoholic fatty liver
667 disease and alters gut microbiota in mice. *World J. Hepatol.* **11**, 619–637 (2019).
668 32. Jiao, N. *et al.* Gut microbiome may contribute to insulin resistance and systemic
669 inflammation in obese rodents: a meta-analysis. *Physiol. Genomics* **50**, 244–254 (2018).
670 33. Petersen, C. *et al.* T cell–mediated regulation of the microbiota protects against obesity.
671 *Science (80-.).* **365**, (2019).
672 34. Golloso-Gubat, M. J. *et al.* Gut Microbiota and Dietary Intake of Normal-Weight and

673 Overweight Filipino Children. *Microorganisms* **8**, 1015 (2020).
674 35. Chen, X. *et al.* Alteration of the gut microbiota associated with childhood obesity by 16S
675 rRNA gene sequencing. *PeerJ* **8**, e8317 (2020).
676 36. Bosshard, P. P., Zbinden, R. & Altwegg, M. Turicibacter sanguinis gen. nov., sp. nov., a
677 novel anaerobic, Gram-positive bacterium. *Int. J. Syst. Evol. Microbiol.* (2002).
678 doi:10.1099/ijs.0.02056-0
679 37. Maki, J. J., Nielsen, D. W. & Looft, T. Complete Genome Sequence and Annotation for
680 Turicibacter sanguinis MOL361 T (DSM 14220). *Microbiol. Resour. Announc.* **9**, (2020).
681 38. Fung, T. C. *et al.* Intestinal serotonin and fluoxetine exposure modulate bacterial
682 colonization in the gut. *Nature Microbiology* (2019). doi:10.1038/s41564-019-0540-4
683 39. Auchtung, T. A. *et al.* Complete genome sequence of Turicibacter sp. strain H121,
684 isolated from the feces of a contaminated germ-free mouse. *Genome Announc.* (2016).
685 doi:10.1128/genomeA.00114-16
686 40. Russell, D. W. The Enzymes, Regulation, and Genetics of Bile Acid Synthesis. *Annu. Rev.*
687 *Biochem.* **72**, 137–174 (2003).
688 41. Guo, C., Chen, W.-D. & Wang, Y.-D. TGR5, Not Only a Metabolic Regulator. *Front.*
689 *Physiol.* **7**, (2016).
690 42. Ridlon, J. M., Kang, D.-J. & Hylemon, P. B. Bile salt biotransformations by human
691 intestinal bacteria. *J. Lipid Res.* **47**, 241–259 (2006).
692 43. Makishima, M. *et al.* Vitamin D Receptor As an Intestinal Bile Acid Sensor. *Science (80-.*
693 *).* **296**, 1313–1316 (2002).
694 44. Lou, D. *et al.* The three-dimensional structure of Clostridium absonum 7α-hydroxysteroid
695 dehydrogenase: new insights into the conserved arginines for NADP(H) recognition. *Sci.*
696 *Rep.* **6**, 22885 (2016).
697 45. Klaver, F. A. & van der Meer, R. The assumed assimilation of cholesterol by Lactobacilli

698 and Bifidobacterium bifidum is due to their bile salt-deconjugating activity. *Appl.*
699 *Environ. Microbiol.* **59**, 1120–1124 (1993).
700 46. Yao, L. *et al.* A selective gut bacterial bile salt hydrolase alters host metabolism. *Elife*
701 (2018). doi:10.7554/elife.37182
702 47. Joyce, S. A. *et al.* Regulation of host weight gain and lipid metabolism by bacterial bile
703 acid modification in the gut. *Proc. Natl. Acad. Sci.* **111**, 7421–7426 (2014).
704 48. Whitaker, W. R., Shepherd, E. S. & Sonnenburg, J. L. Tunable Expression Tools Enable
705 Single-Cell Strain Distinction in the Gut Microbiome. *Cell* **169**, 538-546.e12 (2017).
706 49. Hylemon, P. B. & Sherrod, J. A. Multiple forms of 7-alpha-hydroxysteroid dehydrogenase
707 in selected strains of Bacteroides fragilis. *J. Bacteriol.* **122**, 418–424 (1975).
708 50. Sherrod, J. A. & Hylemon, P. B. Partial purification and characterization of NAD-
709 dependent 7α-hydroxysteroid dehydrogenase from Bacteroides thetaiotaomicron. *Biochim.*
710 *Biophys. Acta - Lipids Lipid Metab.* **486**, 351–358 (1977).
711 51. Marion, S. *et al.* Biogeography of microbial bile acid transformations along the murine
712 gut. *J. Lipid Res.* **61**, 1450–1463 (2020).
713 52. Hofmann, A. F., Hagey, L. R. & Krasowski, M. D. Bile salts of vertebrates: structural
714 variation and possible evolutionary significance. *J. Lipid Res.* **51**, 226–246 (2010).
715 53. Jones, B. V., Begley, M., Hill, C., Gahan, C. G. M. & Marchesi, J. R. Functional and
716 comparative metagenomic analysis of bile salt hydrolase activity in the human gut
717 microbiome. *Proc. Natl. Acad. Sci.* **105**, 13580–13585 (2008).
718 54. Begley, M., Hill, C. & Gahan, C. G. M. Bile Salt Hydrolase Activity in Probiotics. *Appl.*
719 *Environ. Microbiol.* **72**, 1729–1738 (2006).
720 55. Prete, R. *et al.* Beneficial bile acid metabolism from Lactobacillus plantarum of food
721 origin. *Sci. Rep.* **10**, 1165 (2020).
722 56. Tanaka, H., Hashiba, H., Kok, J. & Mierau, I. Bile Salt Hydrolase of Bifidobacterium

723 longum —Biochemical and Genetic Characterization. *Appl. Environ. Microbiol.* **66**,
724 2502–2512 (2000).
725 57. Kim, G.-B., Miyamoto, C. M., Meighen, E. A. & Lee, B. H. Cloning and Characterization
726 of the Bile Salt Hydrolase Genes (bsh) from Bifidobacterium bifidum Strains. *Appl.*
727 *Environ. Microbiol.* **70**, 5603–5612 (2004).
728 58. Ma, D. *et al.* Ketogenic diet enhances neurovascular function with altered gut microbiome
729 in young healthy mice. *Sci. Rep.* **8**, 6670 (2018).
730 59. Gao, X. *et al.* Correlations between α-Linolenic Acid-Improved Multitissue Homeostasis
731 and Gut Microbiota in Mice Fed a High-Fat Diet. *mSystems* **5**, (2020).
732 60. Everard, A. *et al.* Microbiome of prebiotic-treated mice reveals novel targets involved in
733 host response during obesity. *ISME J.* **8**, 2116–2130 (2014).
734 61. Jung, M.-J. *et al.* Chronic Repression of mTOR Complex 2 Induces Changes in the Gut
735 Microbiota of Diet-induced Obese Mice. *Sci. Rep.* **6**, 30887 (2016).
736 62. Huang, J. *et al.* Supplementation of Bacillus sp. DU-106 reduces hypercholesterolemia
737 and ameliorates gut dysbiosis in high-fat diet rats. *Appl. Microbiol. Biotechnol.* **105**, 287–
738 299 (2021).
739 63. Golloso-Gubat, M. J. *et al.* Gut microbiota and dietary intake of normal-weight and
740 overweight filipino children. *Microorganisms* (2020).
741 doi:10.3390/microorganisms8071015
742 64. Caesar, R., Tremaroli, V., Kovatcheva-Datchary, P., Cani, P. D. & Bäckhed, F. Crosstalk
743 between Gut Microbiota and Dietary Lipids Aggravates WAT Inflammation through TLR
744 Signaling. *Cell Metab.* **22**, 658–668 (2015).
745 65. Martinez-Guryn, K. *et al.* Small Intestine Microbiota Regulate Host Digestive and
746 Absorptive Adaptive Responses to Dietary Lipids. *Cell Host Microbe* **23**, 458-469.e5
747 (2018).

748 66. Jones, M. L., Martoni, C. J. & Prakash, S. Cholesterol lowering and inhibition of sterol
749 absorption by Lactobacillus reuteri NCIMB 30242: a randomized controlled trial. *Eur. J.*
750 *Clin. Nutr.* **66**, 1234–1241 (2012).
751 67. Song, Z. *et al.* Taxonomic profiling and populational patterns of bacterial bile salt
752 hydrolase (BSH) genes based on worldwide human gut microbiome. *Microbiome* **7**, 9
753 (2019).
754 68. Russell, B. J. *et al.* Intestinal Transgene Delivery with Native E.
755 coli Chassis Allows Persistent Physiological Changes. *bioRxiv*
756 2021.11.11.468006 (2021). doi:10.1101/2021.11.11.468006
757 69. Jin, M. *et al.* Analysis of the Gut Microflora in Patients With Parkinson's Disease. *Front.*
758 *Neurosci.* **13**, 1184 (2019).
759 70. Barandouzi, Z. A., Starkweather, A. R., Henderson, W. A., Gyamfi, A. & Cong, X. S.
760 Altered Composition of Gut Microbiota in Depression: A Systematic Review. *Front.*
761 *Psychiatry* **11**, (2020).
762 71. Jackson, M. A. *et al.* Gut microbiota associations with common diseases and prescription
763 medications in a population-based cohort. *Nat. Commun.* (2018). doi:10.1038/s41467-
764 018-05184-7
765 72. Ferguson, J. M. SSRI Antidepressant Medications. *Prim. Care Companion J. Clin.*
766 *Psychiatry* **03**, 22–27 (2001).
767 73. Cascade, E., Kalali, A. H. & Kennedy, S. H. Real-world data on SSRI antidepressant side
768 effects. *Psychiatry* (2009).
769 74. Duncan, S. H. Growth requirements and fermentation products of Fusobacterium
770 prausnitzii, and a proposal to reclassify it as Faecalibacterium prausnitzii gen. nov., comb.
771 nov. *Int. J. Syst. Evol. Microbiol.* **52**, 2141–2146 (2002).
772 75. Lynch, J. B. & Sonnenburg, J. L. Prioritization of a plant polysaccharide over a mucus

773 carbohydrate is enforced by a Bacteroides hybrid two-component system. *Mol. Microbiol.*
774 (2012). doi:10.1111/j.1365-2958.2012.08123.x
775 76. Eren, A. M. *et al.* Community-led, integrated, reproducible multi-omics with anvi'o. *Nat.*
776 *Microbiol.* **6**, 3–6 (2021).
777 77. Yoon, S.-H., Ha, S., Lim, J., Kwon, S. & Chun, J. A large-scale evaluation of algorithms
778 to calculate average nucleotide identity. *Antonie Van Leeuwenhoek* **110**, 1281–1286
779 (2017).
780 78. Altschul, S. F. *et al.* Gapped BLAST and PSI-BLAST: A new generation of protein
781 database search programs. *Nucleic Acids Research* (1997). doi:10.1093/nar/25.17.3389
782 79. Hsieh, W.-Y., Williams, K. J., Su, B. & Bensinger, S. J. Profiling of mouse macrophage
783 lipidome using direct infusion shotgun mass spectrometry. *STAR Protoc.* **2**, 100235
784 (2021).
785 80. Su, B. *et al.* A DMS Shotgun Lipidomics Workflow Application to Facilitate High-
786 Throughput, Comprehensive Lipidomics. *J. Am. Soc. Mass Spectrom.* **32**, 2655–2663
787 (2021).
788 81. Schindelin, J. *et al.* Fiji: an open-source platform for biological-image analysis. *Nat.*
789 *Methods* **9**, 676–682 (2012).
790 82. Galarraga, M. *et al.* Adiposoft: automated software for the analysis of white adipose tissue
791 cellularity in histological sections. *J. Lipid Res.* **53**, 2791–2796 (2012).
792 83. Sayin, S. I. *et al.* Gut Microbiota Regulates Bile Acid Metabolism by Reducing the Levels
793 of Tauro-beta-muricholic Acid, a Naturally Occurring FXR Antagonist. *Cell Metab.* **17**,
794 225–235 (2013).
795 84. Takahashi, S. *et al.* Cyp2c70 is responsible for the species difference in bile acid
796 metabolism between mice and humans. *J. Lipid Res.* **57**, 2130–2137 (2016).
797 85. Kolde, R. pheatmap: Pretty Heatmaps. (2019).

86. Team, R. C. R: A language and environment for statistical computing. (2020).

87. Šidák, Z. Rectangular Confidence Regions for the Means of Multivariate Normal Distributions. *J. Am. Stat. Assoc.* **62**, 626–633 (1967).

802 ***Acknowledgments***

803 *Turicibacter* isolates H121, TA25, T46 and T129 were a gift from Thomas Auchtung. 18F6 and
804 1E2 were a gift from Kenya Honda. pWW3837 and *B. thetaiotaomicron* VPI-5482 was a gift
805 from Fatima Enam and Justin Sonnenburg. We would like to thank Alexander Yoon, Gazmend
806 Elezi, and Lauren Seaman for technical assistance with the LC-MS operation and protocols, and
807 Nathan Hwangbo for statistical guidance. This work was supported by funding from the Packard
808 Foundation (E.Y.H.) and Ford Foundation (J.B.L.). E.Y.H. is a New York Stem Cell Foundation
809 – Robertson Investigator. This research was supported in part by The New York Stem Cell
810 Foundation.

811

812 ***Author Contributions***

813 J. B. L., E. L. G, K. C., K. B. Y., J. P. and E. Y. H. conceptualized and planned bacterial and
814 mouse experiments. J. B. L. and K. F. F. designed and performed LC-MS experiments. J. B. L.,
815 T. J., A. A., and J. L. performed isolation and characterization of novel *Turicibacter* isolates. J.
816 B. L. and E. Y. H. wrote manuscript. All authors read and edited final manuscript.

817

818 ***Competing Interests***

819 The authors declare no competing interests. Findings regarding the host effects of *Turicibacter*
820 reported in the manuscript are the subject of provisional patent application 63/288980, owned by
821 UCLA.

822

823 ***Availability of materials***

824 Bacterial strains from this work may be obtained through reasonable request to the
825 corresponding author. Certain materials may be restricted by MTA requirements.

826

827 **FIGURES**

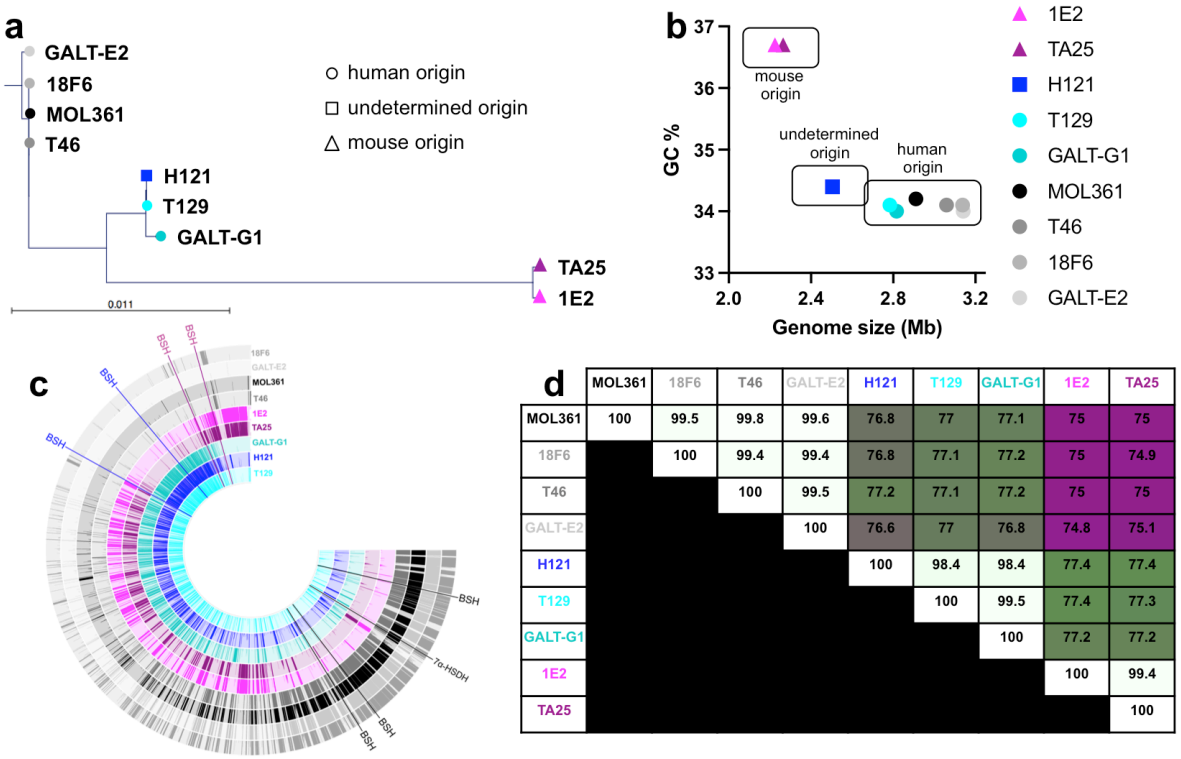

828

829 **Fig. 1. Genomic comparisons reveal distinct subgroups of *Turicibacter*. a**, Phylogenetic tree
830 comparing full-length 16S rRNA gene sequences from noted *Turicibacter* isolates. Circles
831 indicate human-derived isolates, triangles indicate mouse-derived isolates, and square indicates a
832 mouse-derived contaminating isolate. **b**, Association between guanine-cytosine % (GC%) and
833 calculated genome size in megabases (Mb) for shotgun-assembled genomes of *Turicibacter*
834 isolates from **a**. **c**, Full genome sequence comparisons across *Turicibacter* strains. Position of
835 predicted bile-modification gene homologs are noted outside of rings, with the color of the gene
836 name denoting the genome family that gene is found in. Each ring represents sequence blocks in
837 one genome. **d**, Average nucleotide identity (ANI) between noted *Turicibacter* genomes.
838 Number denotes ANI, white-green-maroon scale represents 100%-75% ANI scale.

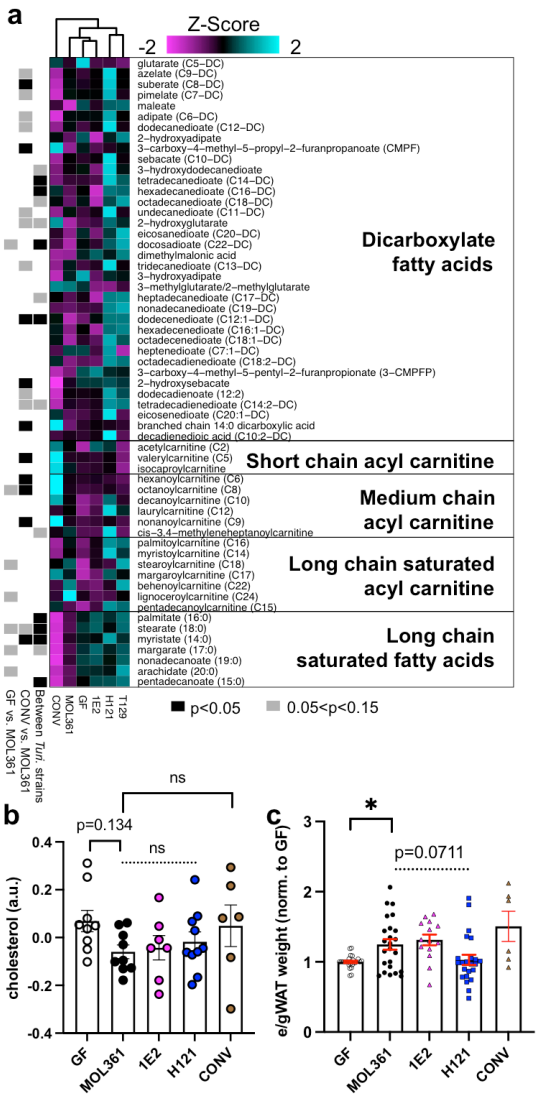

Fig. 2. Colonization with different *Turicibacter* strains alters host lipids . a, Heatmap of relative abundance of serum lipids from gnotobiotic mice monocolonized with noted *Turicibacter* strains. Heatmap values (Z-score) represent mean abundance of each detected lipid species from labeled lipid categories scaled across all the means of that individual lipid species. Black ($p<0.05$) and grey ($0.05<p<0.15$) rectangles indicate statistically significant differences of that metabolite between: left, GF and MOL361 monocolonized mice; middle, CONV and MOL361 monocolonized mice; and right, between MOL361, 1E2, and H121 monocolonized mice. **b**, Serum cholesterol concentrations of mice colonized by noted *Turicibacter* strains. **c**, Sex and litter-matched relative epidydimal/gonadal white adipose tissue (e/g WAT) mass of mice

849 monocolonized with noted *Turicibacter* strains. Shapes indicate value for individual mouse,
850 dotted bar represents ANOVA statistic for groups below the line. Metabolite and cholesterol
851 analysis n=6-10. WAT analysis n=6-26, Mann-Whitney test for MOL361-GF and MOL361-
852 CONV comparisons, Kruskal-Wallis for intra-*Turicibacter* comparison, Šidák correction for
853 multiple comparisons[87]. *$p<0.05$.

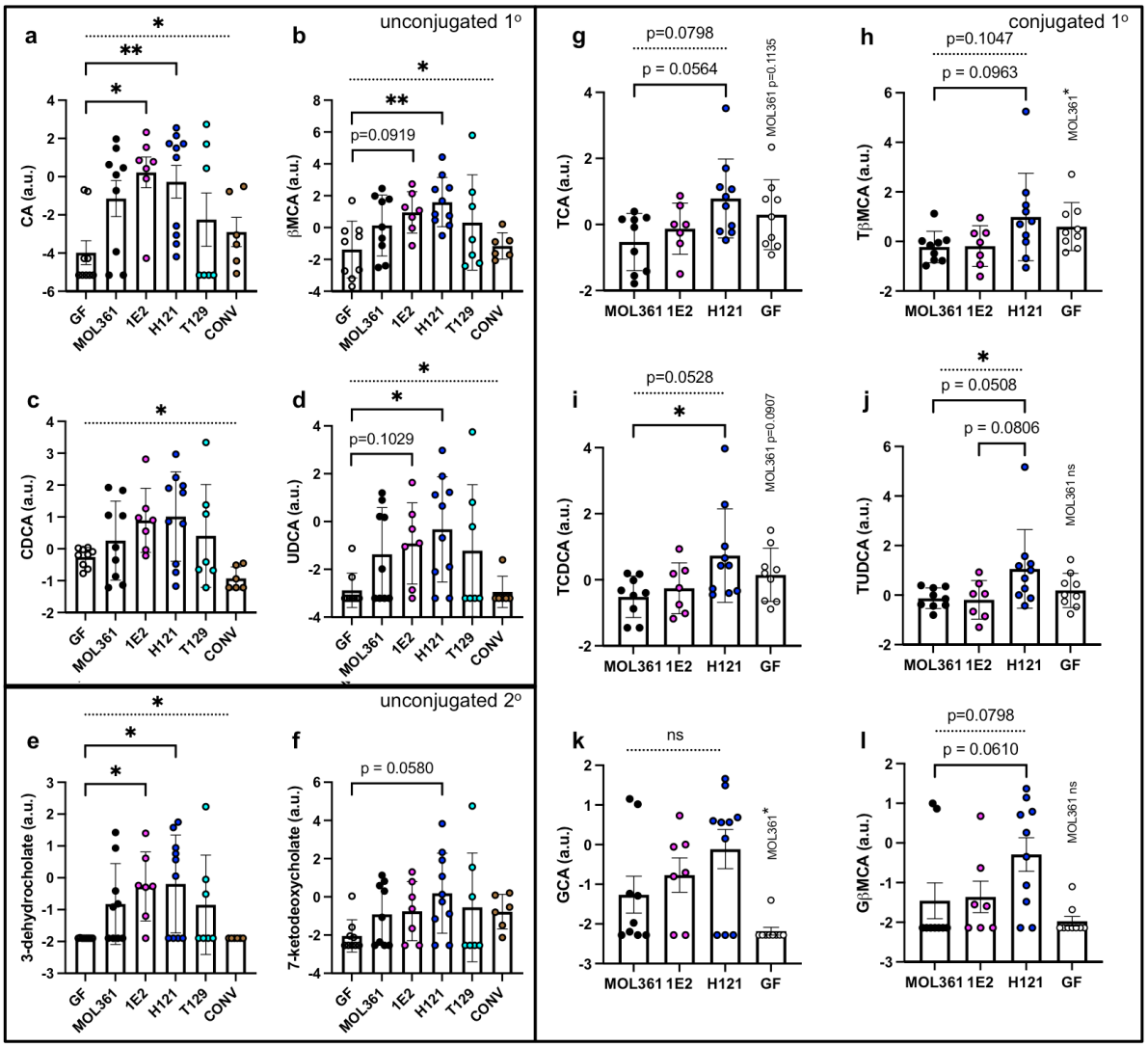

Fig. 3. *Turicibacter* colonization alters circulating host bile species in a strain-specific manner. Serum concentrations of **a-d**, primary unconjugated bile acids; **e-f**, secondary unconjugated bile acids; or **g-l**, primary conjugated bile acids. Points indicate log-transformed value for individual mouse with shapes and colors matching **Fig. 1**, error bars represent mean +/- SEM. Kruskal-Wallis test across all noted colonizations with Dunn's multiple comparisons to GF for **a-f.** Kruskal-Wallis test between noted *Turicibacter* strains and multiple comparisons to H121 for **g-l**. Mann-Whitney test used to compare GF and MOL361 in g-l, and p-values are noted above GF data points. n=6-10 for each group. Dotted bar represents ANOVA statistic for groups below the line. *p<0.05, **p<0.005.

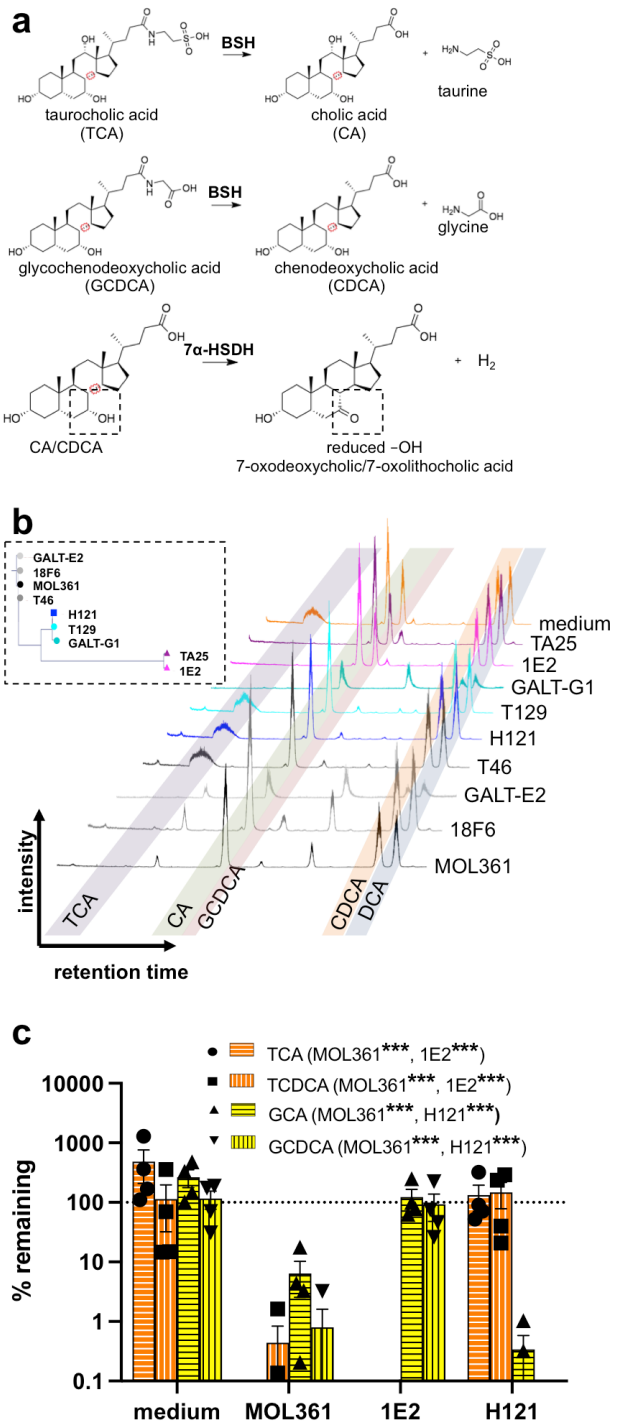

Fig. 4: *Turicibacter* isolates differ in their bile-modifying abilities. a, Schematic for types of bile transformations found to be performed by *Turicibacter* isolates. **b**, inset: 16S rRNA gene-based phylogenic tree from Fig. 1a. Liquid chromatograms of individual *Turicibacter* isolates grown for 24 hours in media with sub-inhibitory concentrations of five bile acids: taurocholic acid (TCA), cholic acid (CA), glycochenodeoxycholic acid (GCDCA), chenodeoxycholic acid

870 (CDCA), and deoxycholic acid (DCA). Shaded regions indicate expected retention time of each
871 bile species. **c**, Percent remaining (compared to cultures at time=0) of conjugated bile acids
872 (TCA, taurochenodeoxycholic acid [TCDCA], glycocholic acid [GCA], GCDCA) after 24
873 growth with noted *Turicibacter* isolate. Yellow=glycine-conjugated bile acids, orange=taurine-
874 conjugated bile acids. n=4 independent cultures. Values not shown were below 0.1% remaining.
875 Statistical analysis performed by one sample t-test, annotations of legend denotes strains with
876 significant difference from 100% remaining for each bile acid.

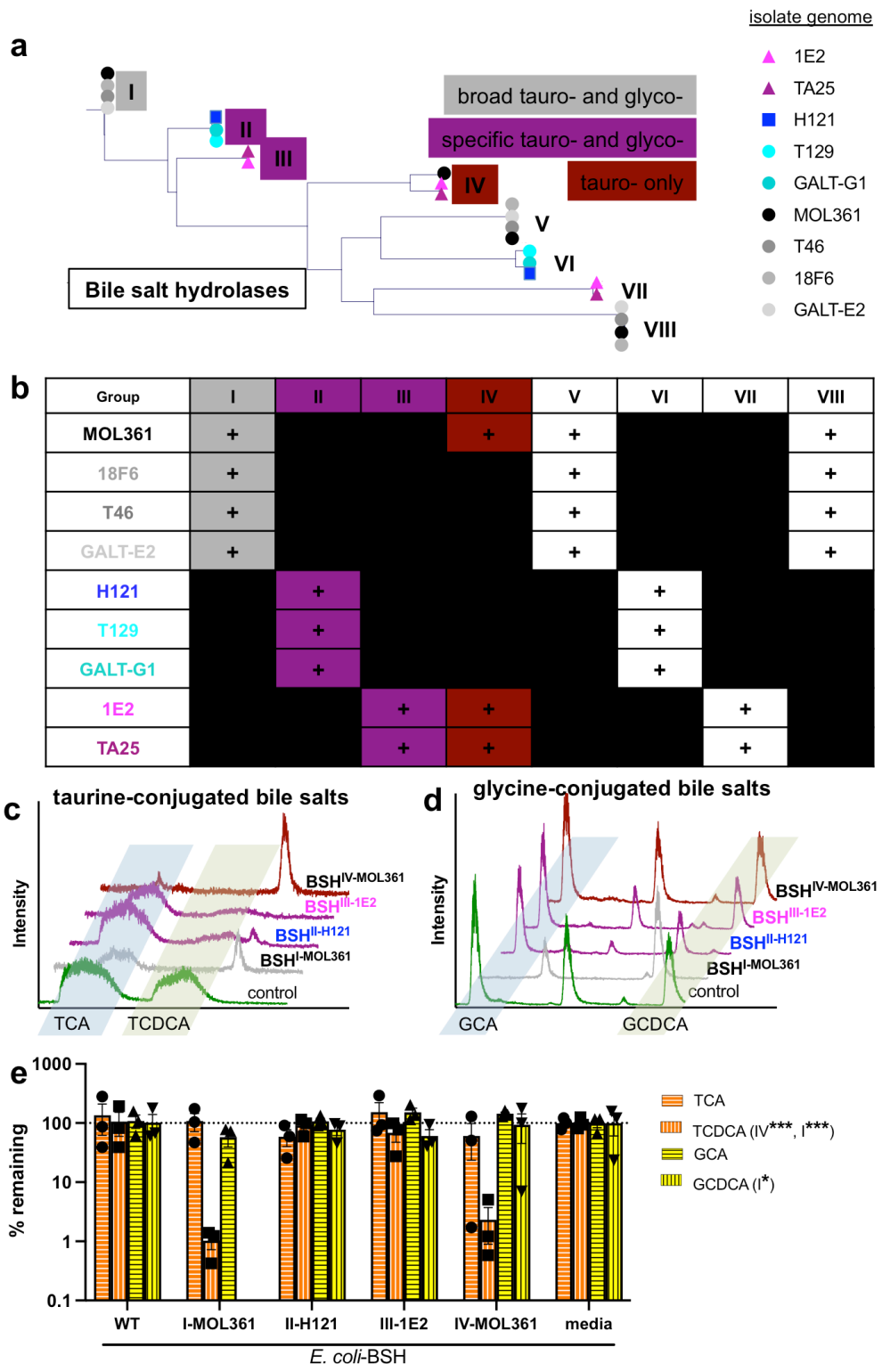

Fig. 5. *Turicibacter* isolates differ in their genetic capacity to modify bile species. a, Phylogenetic tree of amino acid sequences for each predicted bile salt hydrolase (BSH) sequence from *Turicibacter* strains, with observed bile species specificity noted in boxes. We did not

881 detect bile salt hydrolase activity in sequences without boxes, representing groups V-VIII. **b**,
882 Presence (+) or absence of sequence homologs with potential BSH activity in *Turicibacter*
883 strains. **c**, Liquid chromatograms of media after 24 hour cultures of *E. coli* expressing individual
884 predicted *bsh* genes from each sequence grouping and grown in with TCA and TCDCA. Control
885 is *E. coli* with same expression vector but expressing non-bile-modifying gene. **d**, same as **c**, but
886 with GCA and GCDCA instead of tauro-bile acids. **e**, Quantification of percent remaining
887 (compared to media controls) of conjugated bile acid (TCA, TCDCA, GCA, GCDCA) after 24h
888 growth with *E. coli* expressing the noted *Turicibacter bsh* gene. n=3 independent cultures,
889 annotations in legend indicate *$p<0.05$, **$p<0.005$, ***$p<0.0005$ using one sample t-test
890 comparison with 100% remaining. BSH nomenclature indicates homolog group (*e.g.* III) and
891 isolate of origin (*e.g.* MOL361).

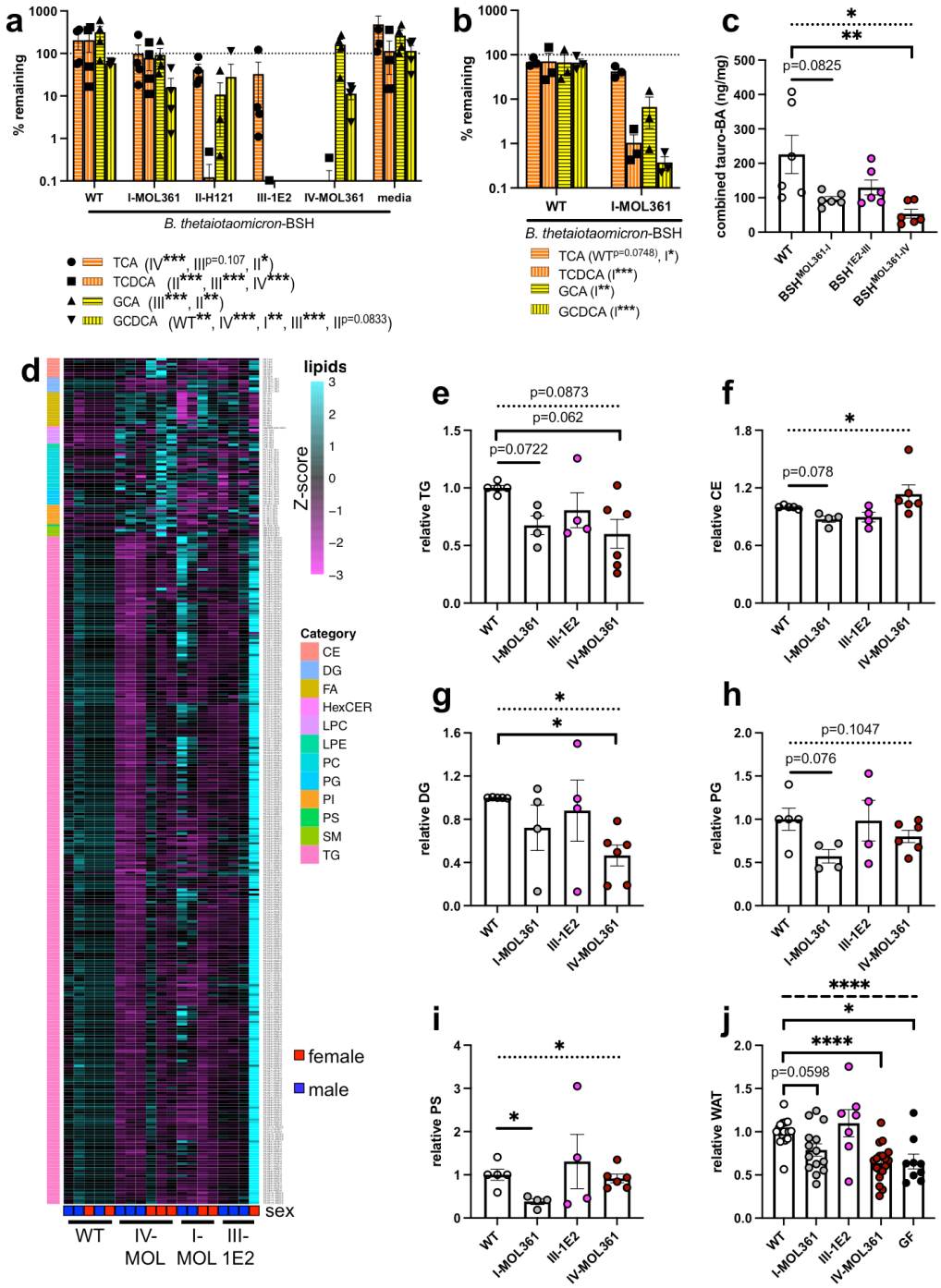

892

893 **Fig. 6: *Turicibacter bsh* expression is sufficient to alter host lipidome and health-associated**

894 **lipid markers. a**, Percent remaining of noted bile acids after 24 hour growth with *Bacteroides*

895 *thetaiotaomicron* expressing noted *bsh* genes. n=4 cultures per strain. **b**, Same as **a**, but with 48

896 hour growth with noted *B. thetaiotaomicron* strains. n=3 cultures per strain. For **a** and **b**, points

897 represent individual comparison with media control, legend annotations denote strains with

898 statistical significance for each bile acid using one sample t-test comparison with 100%
899 remaining. **c**, Quantification of combined taurine-conjugated cecal bile acids (BA) from mice
900 colonized with *bsh*-expressing *B. thetaiotaomicron.* Statistical analysis was performed with
901 Kruskal-Wallis test with Dunn's multiple comparisons test. n=6 animals per colonization. **d**,
902 Heatmap of circulating lipid species significantly altered by expression of at least one
903 *Turicibacter bsh* in *B. thetaiotaomicron*. Heatmap Z-score values represent mean abundance of
904 each detected lipid species from labeled lipid categories scaled across all the means of that
905 individual lipid species. Colors on left correspond to lipid class, each column represents one
906 animal. **e-i**, Relative combined circulating concentrations of **e**, triglycerides (TG), **f**, cholesterol
907 esters (CE), **g**, diacylglycerides (DG), **h**, phosphotidylglycines (PG), or **i**, phosphotidylserines
908 (PS) of mice monocolonized with *bsh*-expressing *B. thetatiotaomicron.* **j**, Relative white adipose
909 tissue weight of mice monocolonized with *bsh*-expressing *B. thetatiotaomicron*. All values in **e-j**
910 normalized to sex-matched littermates, n=4-6 animals per colonization, statistical analysis
911 performed by Welch's ANOVA with Dunnett's multiple comparisons to GF, dotted bar in **c, e-j**
912 represents ANOVA statistic for groups below the line. *$p<0.05$, **$p<0.005$, ***$p<0.0005$.

913 **SUPPLEMENTARY FIGURES**

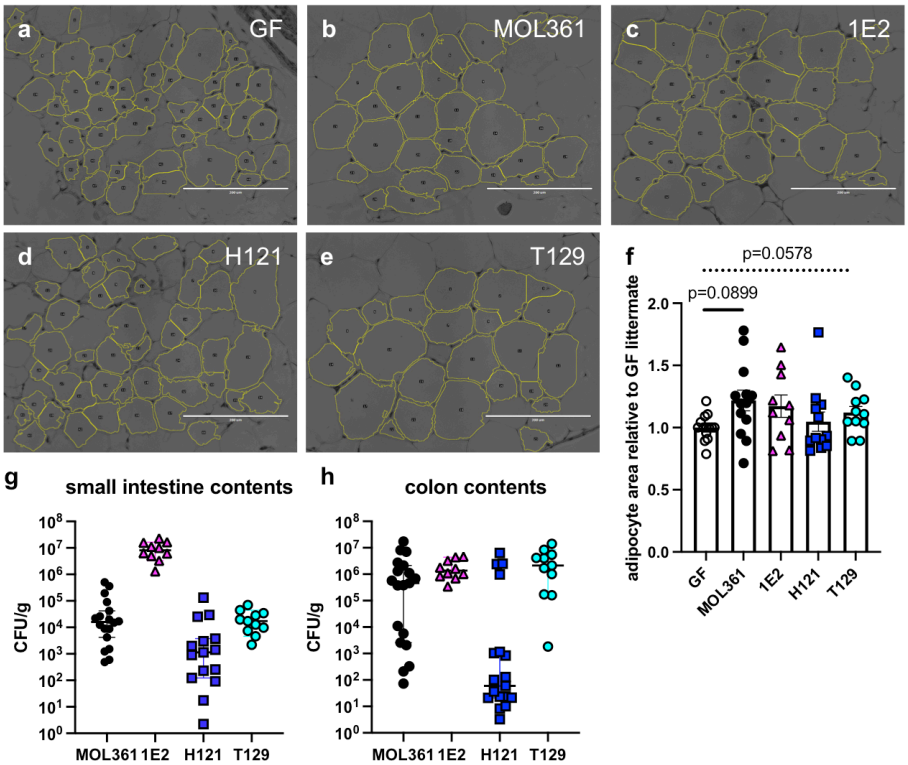

914

915 **Supplementary Fig. 1. Strain-dependent variation in colonization and adipocyte size. a-e**,
916 Representative images of adipose tissue from *Turicibacter* monocolonized mice. **f**, Sex- and
917 litter- matched relative adipocyte area of mice monocolonized with individual *Turicibacter*
918 strains. Each point represents mean of 10 images of adipocyte area per animal. **g, h**, Colony-
919 forming units (CFU) equivalents per gram of contents for distal small intestine (**g**) or proximal
920 colon **(h).** Each dot represents sample from one animal, per colonization n=10-15 for qPCR,
921 n=10-14 for adipocyte area calculation. Statistics for adipocyte area performed by Welch's
922 ANOVA with Dunnet's multiple comparisons, dotted bar represents ANOVA statistic for each
923 group versus the combined experimental mean.

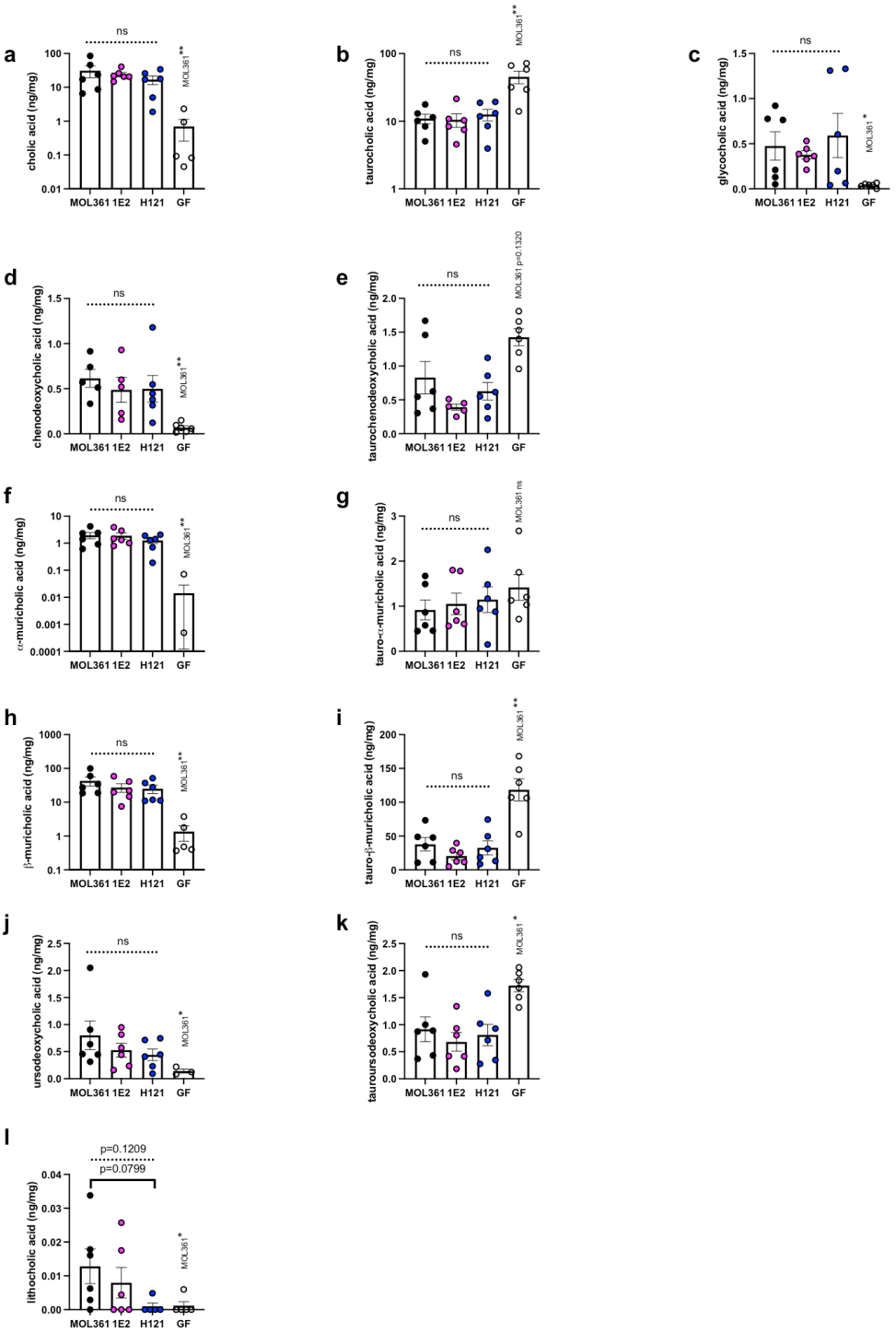

Supplementary Fig. 2. *Turicibacter* colonization alters cecal bile acids. Cecal concentrations of conjugated and unconjugated species of **a-c,** cholic acid, **d-e**, chenodeoxycholic acid, **f-g**, alpha-muricholic acid, **h-i**, beta-muricholic acid, **j-k**, ursodeoxycholic acid, and the unconjugated secondary bile acid **l**, lithocholic acid, in GF or *Turicibacter* monocolonized mice. Each point represents one animal, n=6 animals per condition. Statistical comparisons between *Turicibacter*

930 isolates performed with Kruskal-Wallis test with Dunn's multiple comparisons, GF-MOL361
931 comparisons with Mann-Whitney test. Dotted line represents combined intra-*Turicibacter*
932 ANOVA p-value, value written above GF represents GF-MOL361 p-value, *$p<0.05$, **$p<0.005$.

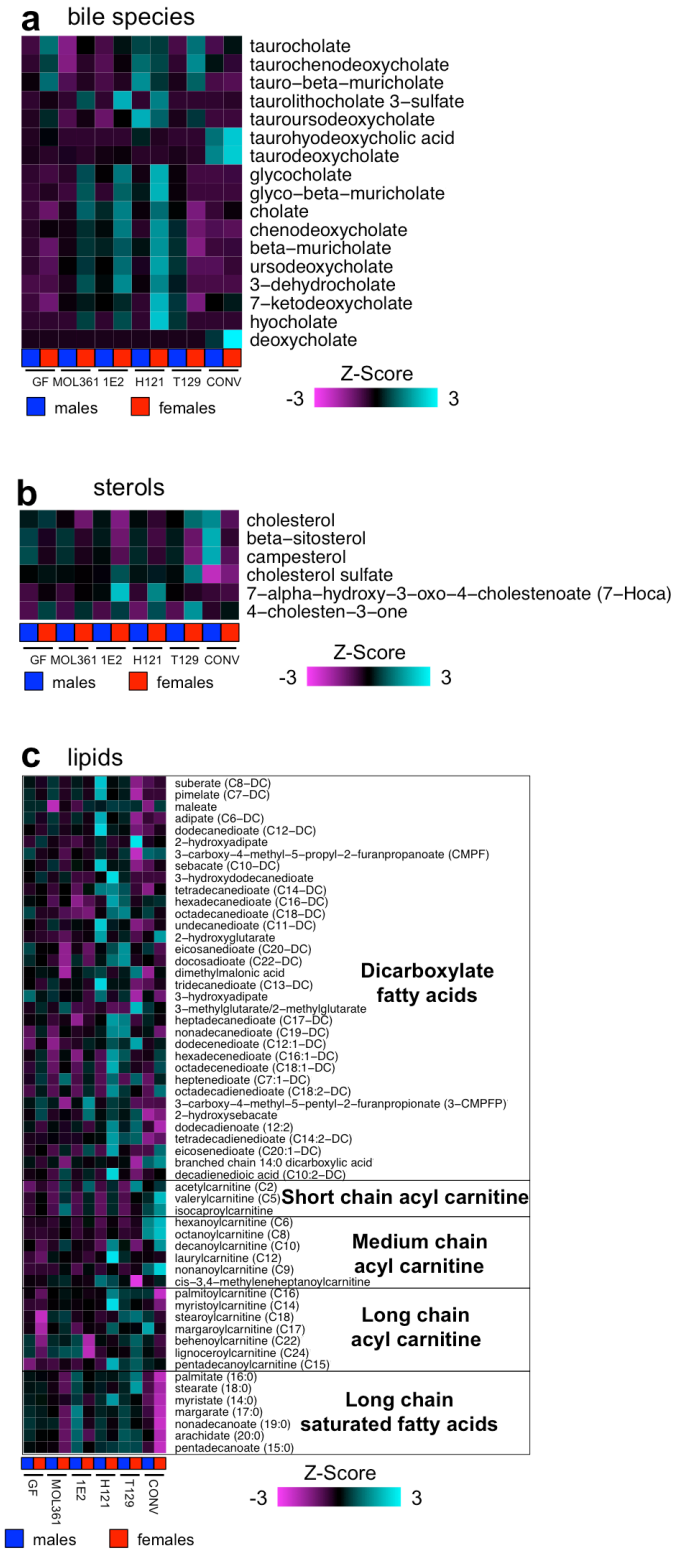

933

934 **Supplementary Fig. S3. Host effects of *Turicibacter* colonization varies with sex. a-c**,

935 Heatmap of mean relative **a**) bile species, **b**) sterols, or **c**) lipids. Column labels represent

936 colonization state and sex, blue=male, red=female. n=3-6 per group, except female T129 (n=1).

	Presence (+) or absence (-) of peak							Deconjugation ability
Turicibacter strain	TCA	Dehydrogenated CA	CA	GCDCA	Dehydrogenated CDCA	CDCA	DCA	
MOL361	-	+	+	-	+	+	+	Tauro- and glyco-deconjugation; dehydrogenation
18F6	-	+	+	-	+	+	+	
GALT-E2	-	+	+	-	+	+	+	
T46	+	-	+	-	-	+	+	Glyco-deconjugation
H121	+	-	+	-	-	+	+	
T129	+	-	+	-	-	+	+	
GALT-G1	-	-	+	-	+	+	+	Tauro- and glyco-deconjugation; some dehydrogenation
1E2	-	-	+	+	-	+	+	Tauro- deconjugation
TA25	-	-	+	+	-	+	+	

Red = outliers from genomic group

Supplementary Fig. 4. Summary table of bile transformations performed by *Turicibacter* isolates. Table indicating presence/absence of noted bile species after growth in mixture of bile acids described in **Fig. 4b**.

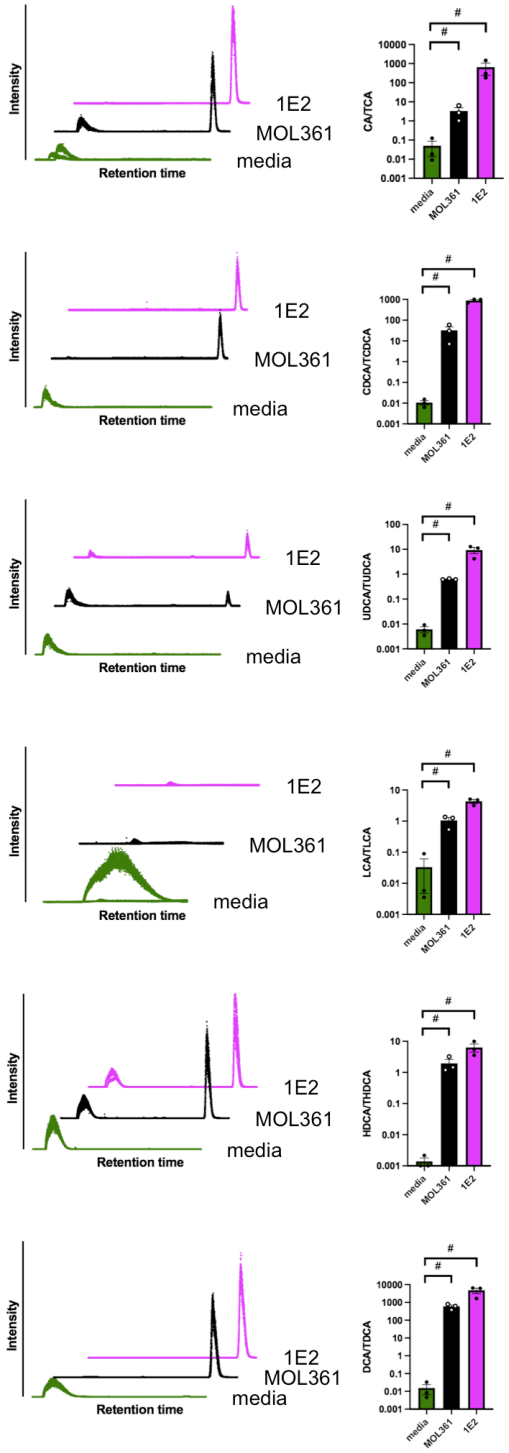

941

942 **Supplementary Fig. 5. *Turicibacter* strains MOL361 and 1E2 can deconjugate at least six**
943 **taurine-conjugated bile acids.** Chromatograms (left) and unconjugated/conjugated bile acid
944 ratios (right) of *Turicibacter* MOL361 or 1E2 grown for 24 hours in YCFA + 0.5mM of
945 individual taurine-conjugated bile acids: **a**, TCA; **b**, TCDCA; **c**, tauroursodeoxycholic acid

946 (TUDCA); **d**, taurolithocholic acid (TLCA); **e**, taurohyodeoxycholic acid (THDCA); **f**,
947 taurodeoxycholic acid (TDCA). Chromatograms are concatenated reconstructed chromatograms
948 for conjugated and unconjugated bile acid. Each trace and each point represents one biological
949 replicate, n=3 cultures. Statistics were performed by Mann-Whitney test, #$p \leq 0.1$ (Note: this p-
950 value is the minimum for this test and our experimental parameters).

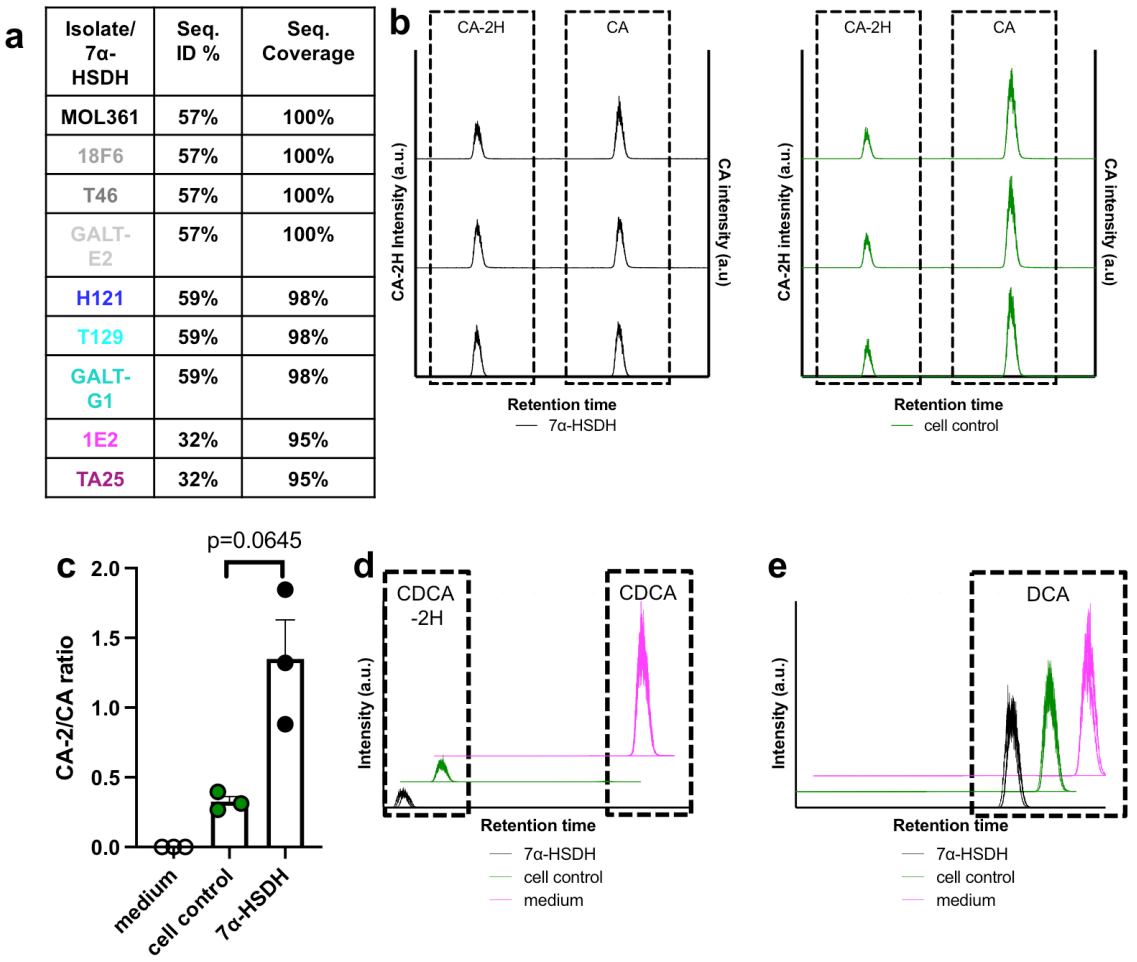

Supplementary Fig. 6. Some strains of *Turicibacter* encode a functional 7alpha-HSDH gene. **a**, Table depicting amino acid similarity and sequence coverage between closest predicted 7alpha-HSDH homolog in noted isolate genome and 7alpha-HSDH gene from *Clostridium absonum*. **b**, Chromatograms of cholic acid (CA) or cholic acid with 2 hydrogens removed (CA-2H) from *E. coli* cultures expressing the MOL361 HSDH homolog (7alpha-HSDH) or non-bile modifying gene sequence in the same plasmid (cell control). Chromatograms from independent triplicate cultures are shown, dotted boxes indicate each bile species. **c**, Quantification of CA/CA-2H ratios determined from reconstructed areas under the curve in **b**. Statistical comparison performed with Welch's t-test, n=3 cultures, bars indicate mean +/- SEM. **d**, Same as **b**, but with CDCA instead of CA. **e**, same as **b**, but with DCA instead of CA. **d** and **e** triplicate chromatograms are stacked on the same axis.

Bile salt hydrolase (*bsh*) gene	Presence (+) or absence (-) of peak				Deconjugation ability
	TCA	TCDCA	GCA	GCDCA	
I-MOL361	-	-	-	-	Tauro- and glyco-deconjugation
II-H121	+	-	+	-	-CDCA deconjugation
III-1E2	+	-	+	+	TCDCA deconjugation
IV-MOL361	-	-	+	+	Tauro- deconjugation

963

964 **Supplementary Fig. 7. Bile transformations performed by *B. thetaiotaomicron* expressing**
965 ***Turicibacter bsh* genes.** Table indicating presence/absence of noted bile species after growth in
966 mixture of bile acids described in **Fig. 6a, b**.

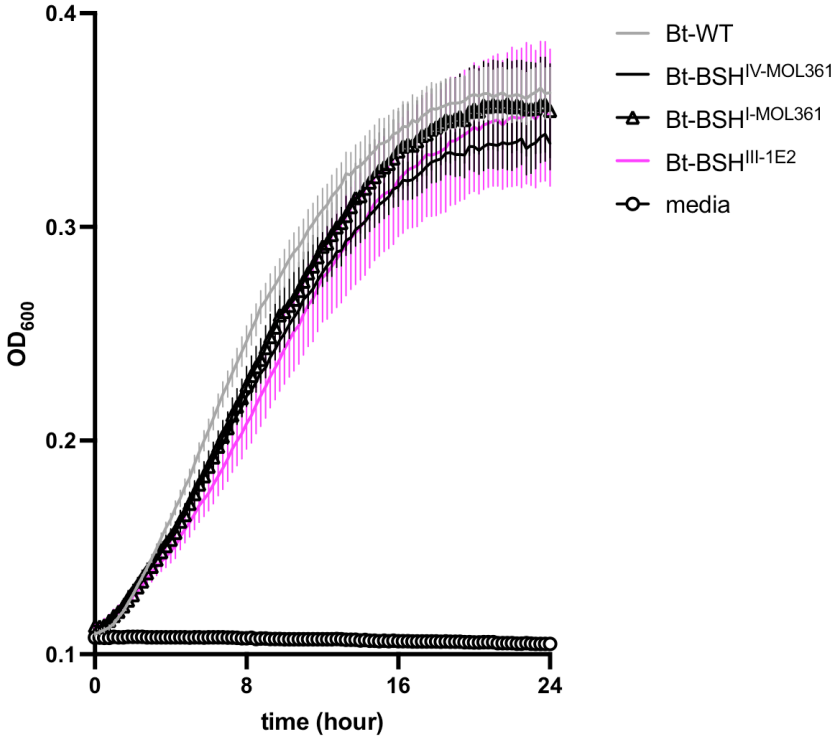

967

968 **Supplementary Fig. 8. Expressing *bsh* genes from *Turicibacter* does not impart significant**

969 ***in vitro* growth defect of *B. thetaiotaomicron*.** OD_{600} readings of noted *B. thetaiotaomicron*

970 strains in BHI-S medium. Each point represents mean +/- SEM for 6 independent cultures.

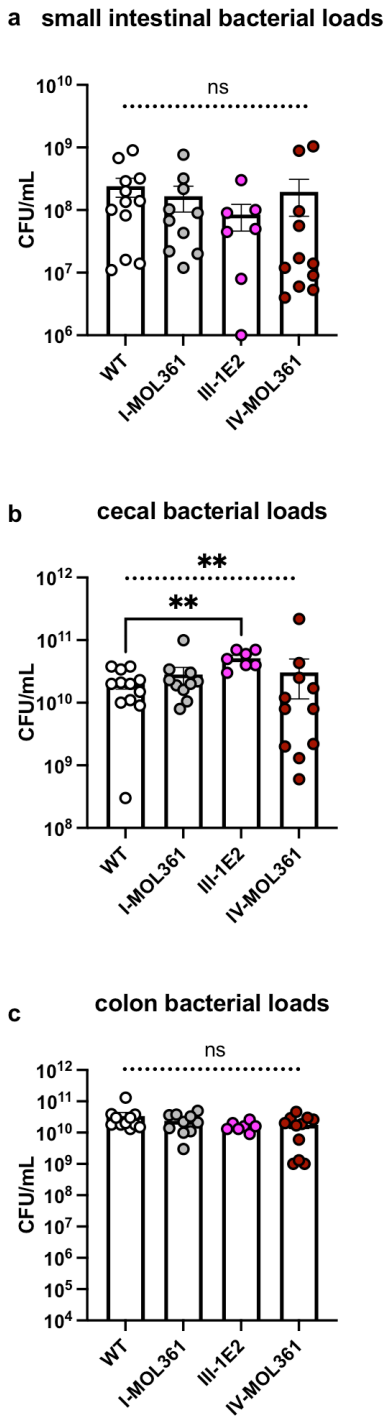

Supplementary Fig. 9. *bsh* expression does not alter *B. thetaiotaomicron* colonization of the murine gut. CFU/mL quantifications of the noted *B. thetaiotaomicron* strains in the **a,** distal small intestine; **b,** cecum and; **c,** proximal colon of gnotobiotic mice. n=7-12/group, comparisons with Welch's ANOVA test and Dunnet's multiple comparisons.

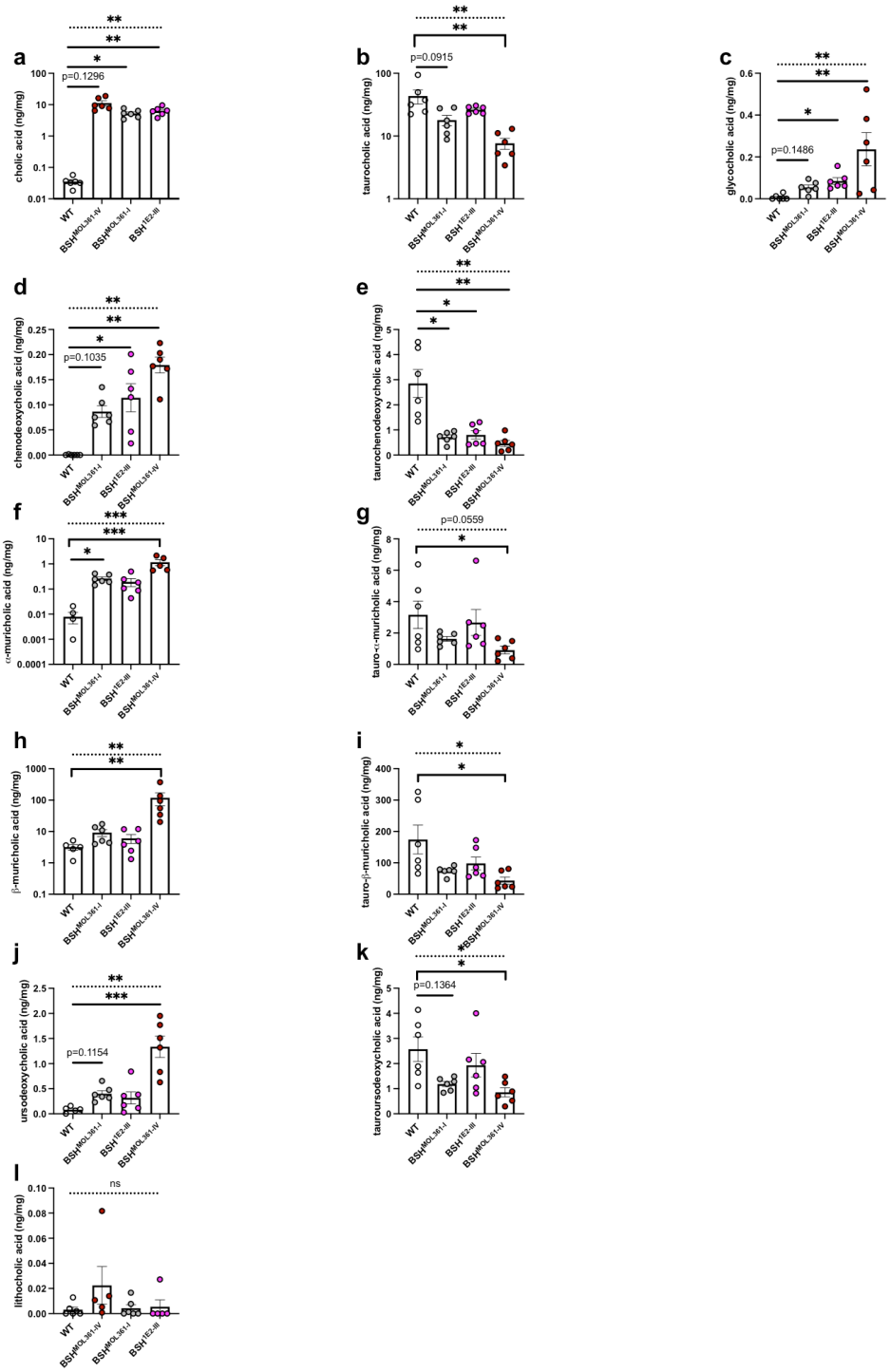

Supplementary Fig. 10. Engineered *B. thetaiotaomicron* transforms host bile acids *in vivo*. Cecal abundance of unconjugated and conjugated species of primary bile acids **a-c,** cholic acid, **d-e**, chenodeoxycholic acid, **f-g**, alpha-muricholic acid, **h-i**, beta-muricholic acid, **j-k**, ursodeoxycholic acid, and the unconjugated secondary bile acid **l**, lithocholic acid. n=3 (3 males, 3 females) for each condition. Statistics performed with Kruskal-Wallis test with Dunn's

982 multiple comparisons. Dotted horizontal line represents total ANOVA statistic across all four

983 groups, *$p<0.05$, **$p<0.005$, ***$p<0.0005$.

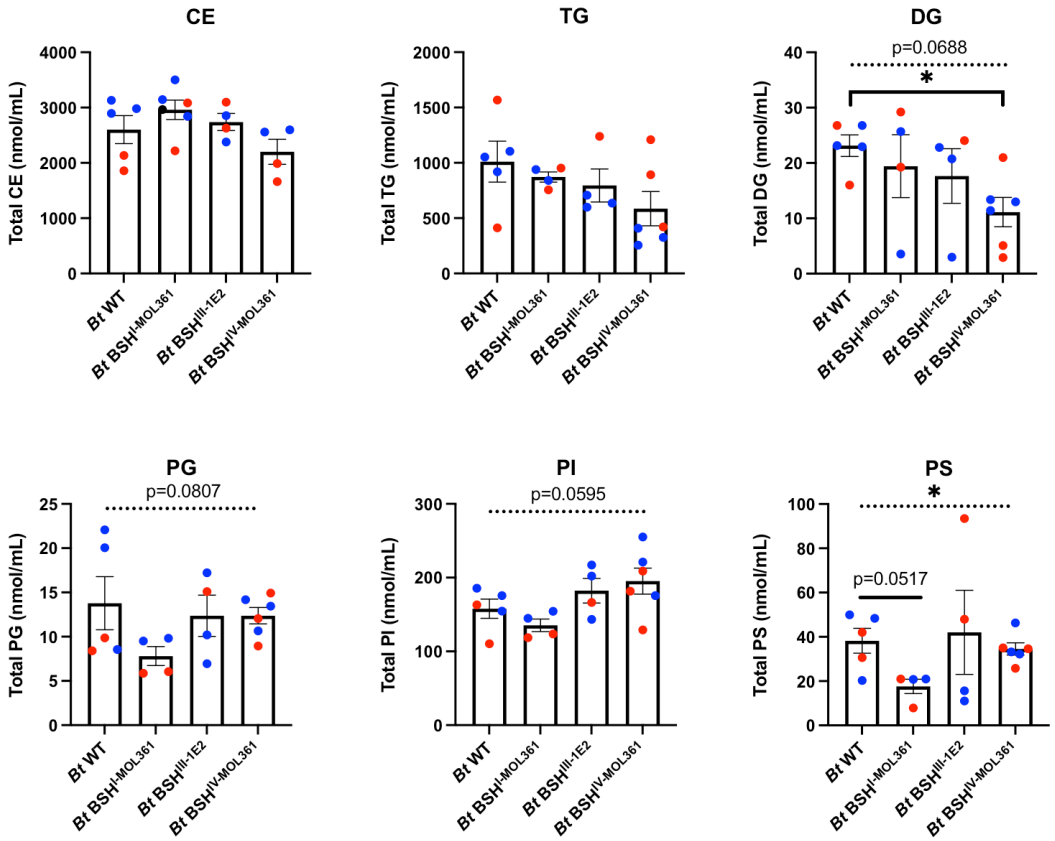

Supplementary Fig. 11. *Turicibacter bsh* expression by *B. thetaiotaomicron* is sufficient to drive broad scale changes in circulating host lipids in male and female mice. Related to **Fig. 6e-j**, circulating absolute concentrations of specific lipid categories in mice colonized by *B. thetaiotaomicron* expressing the noted *Turicibacter bsh* homologs. Each point represents one animal, red points indicate female, blue represent male. n=4-5 per colonization, error bars represent mean +/- SEM. Statistical comparison done with Welch's ANOVA with Dunnett's multiple comparisons, dotted bar represents ANOVA statistic for all four groups, *p<0.05.

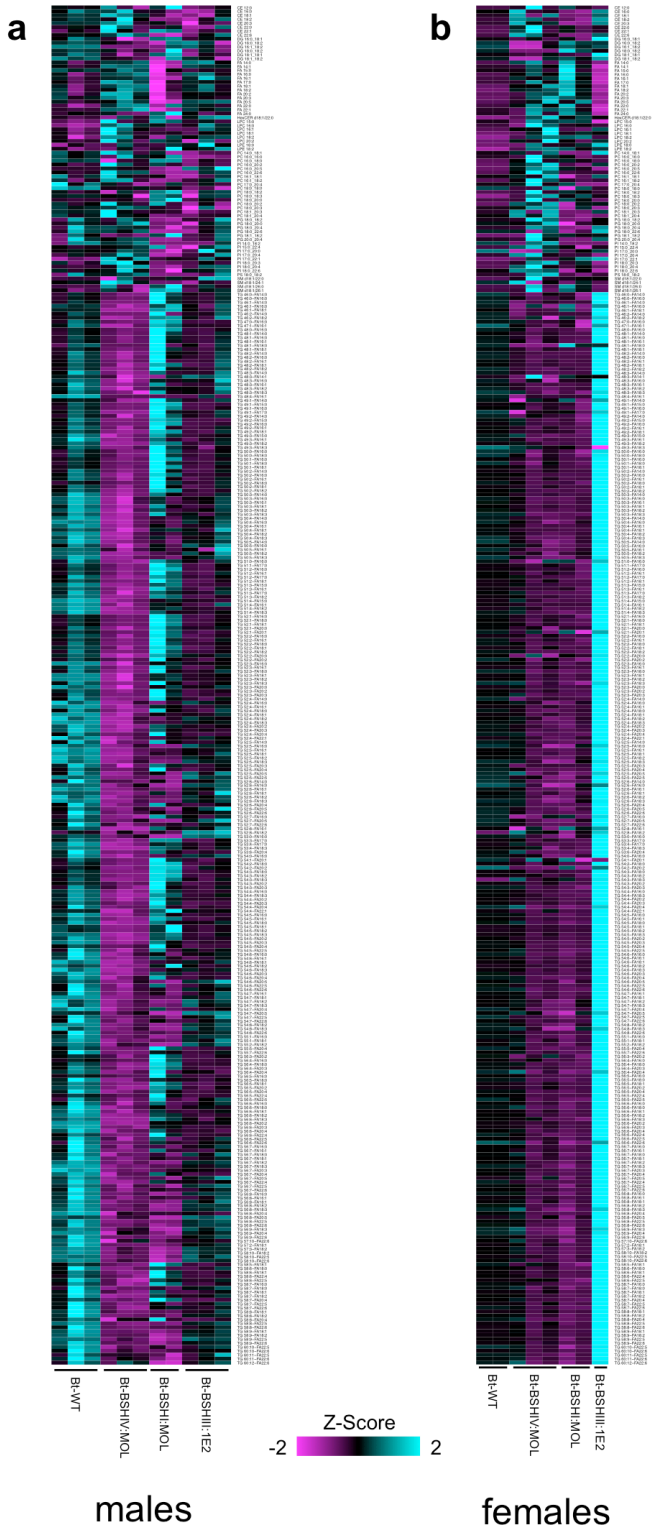

992

993 **Supplementary Fig. 12. Sex differences in lipidomic response to *Turicibacter bsh* expression**

994 **in *B. thetaiotaomicron***. Similar to **Fig. 5b**, but animal lipidome analysis separated into **a**) males

995 and **b**) females. Note that lipid species presented were found to be significantly altered by

expression of at least one *bsh* in males and females combined (i.e. all lipid species shown across the three analyses are the same). Each column represents one animal.

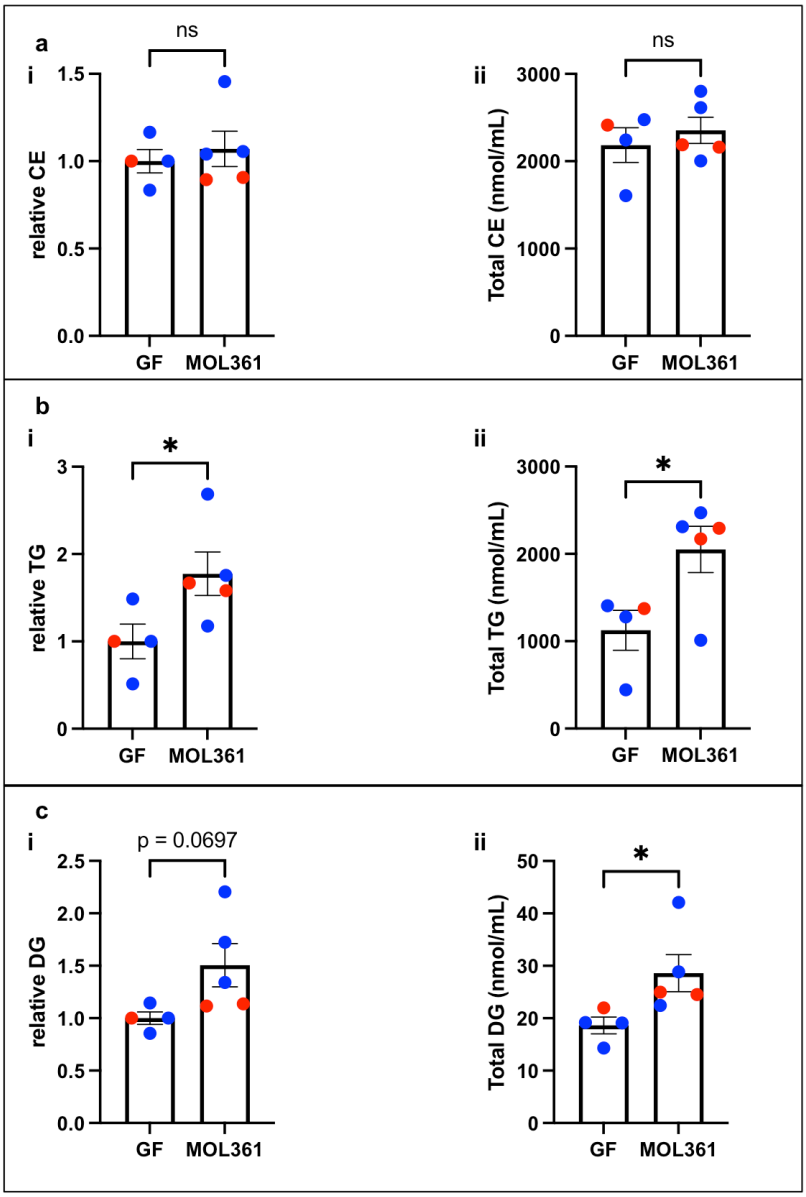

Supplementary Fig. 13. *T. sanguinis* MOL361 colonization leads to increased triglycerides and diacylglycerides, consistent with adipose tissue increases. Plasma levels of combined **a**, cholesterol esters, **b,** triglycerides, and **c,** diacylglycerides. **i:** relative to sex-matched GF littermates, **ii**: absolute quantification. n=4-5 (1-2 females, 3 males per condition). red=female, blue=male. Statistical comparisons Student's two tailed t-test with Welch's correction, *p<0.05.

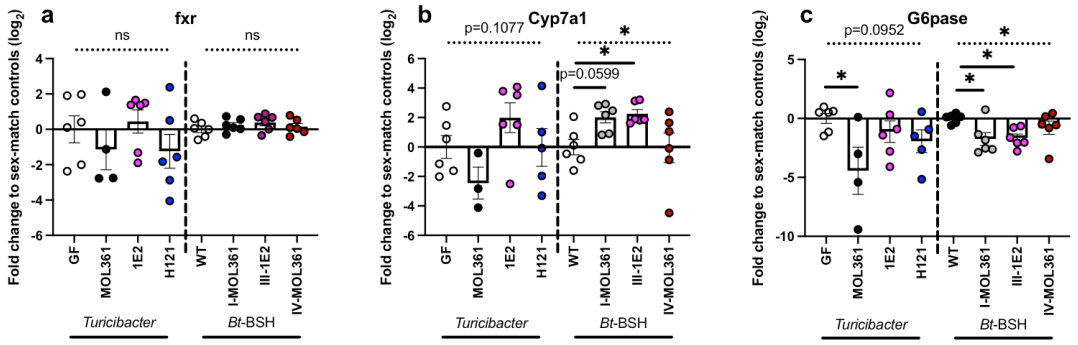

1004

1005 **Supplementary Fig. 14. *Turicibacter* colonization and *bsh* expression induce similar gene**
1006 **expression patterns in the liver.** qRT-PCR analysis of liver transcript levels of **a,** Fxr; **b,**
1007 Cyp7a1; and **c,** G6pase after colonization with the noted *Turicibacter* strains or *B.*
1008 *thetaiotaomicron* expressing the noted *bsh* gene. Data are displayed as fold change relative to
1009 appropriate control (GF for *Turicibacter* colonizations, *Bt*-WT for *bsh* colonizations). Each point
1010 represent data from a single animal, statistics performed with Kruskal-Wallis test with Dunn's
1011 multiple comparisons. Dotted horizontal line represents ANOVA statistic for that comparison of
1012 groups below the line, *p<0.05.

1013

1014 **Supplementary Table 1. List of strains used in this work.**
1015

1016 **Supplementary Table 2. Serum metabolomics from GF, CONV, and *Turicibacter***
1017 **monocolonized mice.** Volume-adjusted log-transformed levels of listed serum metabolites from
1018 mice from different colonization states. Raw p-values generated from Mann-Whitney U test (GF-
1019 MOL361 and MOL361-CONV) or Kruskal-Wallis (MOL361-1E2-H121) test. Adjusted p-values
1020 represent p-values with Šidák correction for number of tests of that metabolite.
1021

1022 **Supplementary Table 3. Raw and normalized e/g WAT values for *Turicibacter* and *B.***
1023 ***thetaiotaomicron*-colonized mice.**
1024

1025 **Supplementary Table 4. Absolute quantification of lipid species from plasma of mice**
1026 **colonized with *B. thetaiotaomicron* engineered to express *Turicibacter bsh* genes, GF mice,**
1027 **or MOL361 monocolonized mice.** Raw p-values generated from Student's t-test comparison
1028 with Bt-WT for *Bacteroides* conditions or comparison between GF and MOL361. Adjusted p-
1029 values represent p-values with Šidák correction for number of tests of that lipid.
1030

1031 **Supplementary Table 5. List of oligos used in the work.**